Graduate School ETD Form 9
(Revised 12/07)

PURDUE UNIVERSITY
GRADUATE SCHOOL
Thesis/Dissertation Acceptance

This is to certify that the thesis/dissertation prepared

By Evan Robert Himes

Entitled
The Role of STAT3 in Osteoclast Mediated Bone Resorption

For the degree of Master of Science

Is approved by the final examining committee:

Jiliang Li
Chair

Robert Yost

Melissa Kacena

To the best of my knowledge and as understood by the student in the *Research Integrity and Copyright Disclaimer (Graduate School Form 20)*, this thesis/dissertation adheres to the provisions of Purdue University's "Policy on Integrity in Research" and the use of copyrighted material.

Approved by Major Professor(s): Jiliang Li

Approved by: Simon Atkinson 07/09/2013
Head of the Graduate Program Date

THE ROLE OF STAT3 IN OSTEOCLAST MEDIATED BONE RESORPTION

A Thesis

Submitted to the Faculty

of

Purdue University

by

Evan Himes

In Partial Fulfillment of the

Requirements for the Degree

of

Master of Science

August 2013

Purdue University

Indianapolis, Indiana

For my family

ACKNOWLEDGEMENTS

I would like to thank my advisor Dr. Jiliang Li for all his help and guidance and my committee members: Dr. Melissa Kacena and Dr. Robert Yost. I would also like to thank Dr. Kacena and her lab for their help with the osteoclast cell culture, Dr. Keith Condon and Yongqi Yu for their help with histology, Kevin Zhou for his guidance, Tomas Meijome and Ryne Horn for their help with osteoclast isolation and mechanical testing, and all other members of Dr. Li's lab, including Kimberly Ho-A-Lim, Layla Mihuti, Samantha Lenz, Tiffany Riddle, and Lindsay Egan.

TABLE OF CONTENTS

Page

LIST OF TABLES vii
LIST OF FIGURES viii
LIST OF ABBREVIATIONS x
ABSTRACT xiii
CHAPTER 1. INTRODUCTION 1
1.1 Skeletal Structure 1
1.2 Bone Macroscopic Anatomy 1
1.3 Bone Modeling 3
1.4 Bone Remodeling 3
1.5 Bone Cells 4
1.6 The Osteoclast 5
1.7 Enzymes Involved in Bone Resorption 7
1.7.1 Cathepsin K (CTSK) 7
1.7.2 Tartrate Resistant Acid Phosphatase (TRAP) 7
1.8 Osteoclast Regulation 7
1.9 Bone Biomechanics 8
1.10 Hyper-IgE Syndrome 9
1.11 Signal Transducers and Activators of Transcription 10
1.12 JAK-STAT Pathway 11
1.13 STAT3 Structure 11
1.14 STAT3 Activation 13
1.15 STAT3 Localization 14
1.16 Regulators of STAT3 14
1.17 STAT3 Knockout Mouse Model 15

Page

1.18 STAT3 in Bone 15
1.19 Research Goals 16
CHAPTER 2. MATERIALS AND METHOD 17
2.1 Conditional STAT3 Knockout Mice 17
2.2 PCR for STAT3 and Cre Genes 18
2.3 Immunohistochemistry 19
2.4 Bone Mineral Density (PIXImus) 20
2.5 Mechanical Testing 20
2.6 Micro CT 21
2.7 Osteoclast Cell Culture 21
2.8 Histology 22
2.8.1 Tartrate Resistant Acid Phosphatase (TRAP) Stain 22
2.8.2 VKM Stain 23
2.9 Histomorphometry 23
2.10 Statistics 24
CHAPTER 3. RESULTS 25
3.1 Verification of Osteoclast Specific Knockout Mice 25
3.2 Comparison of Mouse Body Weight and Femur Length 25
3.3 CTSK Specific Knockout Female Mice Decrease in BMD 26
3.4 CTSK Specific KO Mice Trabecular Bone at 8 Weeks Old 26
3.5 CTSK Specific KO Mice Trabecular Bone 16 Week of Age 27
3.6 CTSK Specific KO Increases the Number of Osteoclasts 28
3.7 CTSK Specific STAT3 KO Trabecular BFR at 8 Weeks Old 28
3.8 Cortical Bone Size and Growth Rate in STAT3 KO Mice 29
3.9 Mechanical Testing: 3 Point Bending 29
3.10 Osteoclast Cell Culture 30
CHAPTER 4. DISCUSSION 31
4.1 Decreased Osteoclast Number in STAT3 KO 31
4.2 Osteoclast Number and BV/TV in Trabecular Bone 31
4.3 Differences in Bone Phenotypes at age 8 and 16 Weeks 32

Page

4.4 Males Exhibit Stronger Cortical Bone In STAT3 KO 33
4.5 Future Plans 33
LIST OF REFERENCES 35
TABLES 40
FIGURES 41

LIST OF TABLES

Table Page

Table 1 Abbreviations and formulas for parameters used in cortical bone 40

Table 2 Abbreviations and formulas for parameters used in trabecular bone 41

LIST OF FIGURES

Figure Page

Figure 1: Osteons 42

Figure 2: Bone remodeling units 43

Figure 3: Stress-stain curve and force-displacement curve 44

Figure 4: STAT3 activation 45

Figure 5: STAT3 crystalline structure 46

Figure 6: Membrane receptors for IL-6 family cytokines 47

Figure 7: Determination of mouse genotype 48

Figure 8: Mechanical testing 49

Figure 9: Immunohistochemical staining 50

Figure 10: Body weights of osteoclast specific Stat3 mice 51

Figure 11: Femur length of osteoclast specific STAT3 KO mice 52

Figure 12: BMD and BMC of 8 week CTSK STAT3 KO mice 53

Figure 13: BMD and BMC of adult CTSK mice 54

Figure 14: BMD and BMC of 8 week old TRAP STAT3 KO mice 55

Figure 15: Trabecular bone structure of 8 week old CTSK mice 56

Figure 16: Trabecular bone structure of 16 week old CTSK mice 57

Figure 17: TRAP stain CTSK specific STAT3 KO mice 58

Page

Figure 18: TRAP stain TRAP specific STAT3 KO mice 59

Figure 19: Dynamic histomorphometry CTSK mice 60

Figure 20: Dynamic histomorphometry TRAP mice 61

Figure 21: Cortical bone properties 8 week old CTSK STAT3 mice 62

Figure 22: Mechanical testing of CTSK mouse femur 63

Figure 23: Osteoclast cell culture data 64

LIST OF ABBREVIATIONS

ACP: Avidin-conjugated peroxidase

ARIP: Activin receptor interacting protein 1

BMC: Bone mineral content

BMD: Bone mineral density

BRU: Bone Remodeling Unit

BMP: Bone morphogenic protein

CNTF: Ciliary neurotrophic factor

CT-1: Cardiotrophin-1

CTSK: Cathepsin K

Dlx5: Distal-less homeobox 5

DNA: Deoxyribonucleic acid

EGF: Epidermal growth factor

EDTA: Ethylenediaminetetraacetic acid

FBS: Fetal bovine serum

FCS: Fetal calf serum

FGF: Fibroblast growth factor

GAS: Gamma Activated Sequences

gp130: Glycoprotein 13

GTP: Guanosine triphosphate

HIES: Hyper-IgE Syndrome

H_2O_2: Hydrogen peroxide

IACUC: Institutional Animal Care and Use Committee

IFN: Interferon

IgE: Immunoglobulin E

IL: Interleukin

JAB: JAK-binding protein

JAK: Janus Kinase

KCl: Potassium Chloride

LIF: Leukemia Inhibitory Factor

M-CSF: Macrophage colony-stimulating factor

MMP: Matrix metalloproteinase

NP-40: Nonyl phenoxypolyethoxylethanol

OPG: Osteoprotegrin

OSM: Oncostatin M

PBS: Phosphate buffered saline

PCR: Polymerase chain reaction

PDGF: Platelet-derived growth factor

PIAS: Protein inhibitors of activated STAT

RANKL: Receptor activator of nuclear factor kappa-B ligand

RGD: Arginine-Glycine-Aspartic acid

ROS: Reactive oxygen species

Runx2: Runt-related transcription factor 2

SH2: Src Homology 2

siRNA: Small interfering ribonucleic acid

SOCS: Suppressors of cytokine signaling

SSI: STAT-induced STAT inhibitor

STAT: Signal transducer and activator of transcription

TGF: Transforming growth factor

TRAP: Tartrate-resistant acid phosphatase

Tyk2: Non-receptor tyrosine-protein kinase

VKM: Von Kossa Method with MacNeal's Tetrachrome Counterstain

μCT: Micro-computed tomography

αMEM: α Minimal essential medium

ABSTRACT

Himes, Evan R. M.S., Purdue University, August 2013. The Role of STAT3 in Osteoclast Mediated Bone Resorption. Major Professor: Jiliang Li.

Signal Transducer and Activator of Transcription 3 (STAT3) is known to be related to bone metabolism. Mutation of STAT3 causes a rare disorder in which serum levels of IgE are elevated. This causes various skeletal problems similar to osteoporosis.

To examine the effect of STAT3 in the osteoclast, we obtained two osteoclast specific STAT3 knockout mouse models: one using the CTSK promoter to drive Cre recombinase and another using a TRAP promoter. Examination of these mice at 8 weeks of age revealed a decreased trabecular bone volume in CTSK specific STAT3 knockout mice along with a slight decrease in osteoclast number in both CTSK and TRAP specific STAT3 knockout females. We also noticed changes in bone mineral density and bone mechanical strength in females. These data suggest that STAT3 plays a part in the function of the osteoclast.

CHAPTER 1. INTRODUCTION

1.1 Skeletal Structure

The skeleton of the adult human is made up of 206 bones carrying out various tasks, such as providing a framework to move and support the body, protection of vital organs, and playing a part in mineral homeostasis. Bones may be divided into several groups, including long bones such as those found in the limbs (femur, humerus) and flat bones such as the bones of the skull. The long bones are further divided into the epiphysis, metaphysis, and diaphysis. The diaphysis is a long and hollowed out shaft that spans most of the bone. The metaphysis is the portion of bone between the diaphysis and the growth plate, while the epiphysis is the region beyond the growth plate at each end of the bone [1].

1.2 Bone Macroscopic Anatomy

The inner and outer surfaces of bone are covered in fibrous sheaths. The outer surface is covered in the periosteum, with the exception of areas where joints are located. The periosteum is anchored to the underlying bone by collagenous fibers called

Sharpey's fibers. The periosteum contains the blood vessels and nerves running to the bone, along with osteoblasts and osteoclasts, two cells responsible for building up and breaking down of bone tissue, respectfully.

The endosteum covers the inner surface of the bone and similar to the periosteum, the endosteum also contains blood vessels, nerves, osteoblasts, and osteoclasts. Volkman's canals and Haversian canals which contain blood vessels run through the bone [1].

All bone is arranged in two different formats, cortical bone and cancellous or trabecular bone. Overall, the human skeleton contains more cortical bone than trabecular bone, but this can vary between different locations of the skeleton. Cortical bone appears to be very dense while trabecular bone appears to be a network of rods running between the cortical bone. Both cortical and trabecular bone is made up of the same basic functional unit: the osteon. Osteons are arranged into Haversian systems in cortical bone and saucers in trabecular bone. **(**Figure 1**)** The Haversian systems form cylinders running the length of cortical bone and are made of concentric circles of lamellae. In trabecular bone, the lamellae are stacked together to form saucer-shaped osteons. [1]

The extracellular matrix of bone is composed of a protein network and a mineral component. The organic protein component gives the bone elasticity, while the mineral gives the bone strength. The majority of the protein in bone is type 1 collagen, which is made from two α1 chains and one α2 chain. [2] Smaller amounts of type III and V collagens are also present. [3] The remaining 10-15% of the protein component is made of non-collagenous proteins. About ¼ of these are exogenously made serum proteins that have an affinity for hydroxyapatite. [4] The remaining non-collagenous proteins are

broken into four groups: proteoglycans, glycosylated proteins, glycosylated proteins with cell attachment properties, and γ-carboxylated proteins. The mineral component makes up between 50-70% of bone in an adult and is composed of hydroxyapatite, $[Ca_{10}(PO_4)_6(OH)_2]$. This mineral is initially deposited in sites left open by the collagen fibrils. These crystals become larger as the bone matures and aggregate as they increase in size. [5-7]

1.3 Bone Modeling

Bone structure can be changed through two different processes: modeling and remodeling. In bone modeling, the osteoblasts or osteoclasts shape the bone through either resorption or formation. As an example, the continuous use of an arm can change the size of the radius in tennis athletes. [8] Bone modeling is more common among children who are still growing than in adults. In remodeling, bone resorption and formation are coupled. This involves the breakdown of bone by osteoclasts immediately followed by new bone formation by osteoblasts. [1]

1.4 Bone Remodeling

Remodeling is broken down into 4 phases: activation, resorption, reversal, and formation. The cells involved in this process arrange themselves in a bone remodeling unit, or BRU **(**Figure 2**)**. [9] During activation, mononucleated osteoclast precursors are recruited and fused into multinucleated cells. These preosteoclasts attach to the bone via integrins,

forming a sealed environment within which they can degrade the bone matrix. [10] Destruction of the bone matrix by the osteoclasts begins after activation and is explained below. Reversal begins after the death of the osteoclasts. The bone is covered by a variety of cells during this phase, including monocytes, exposed osteocytes, and preosteoblasts. [1]

During formation, osteoblasts first synthesize a protein matrix and then regulate mineral deposition through secretion of membrane vesicles. These vesicles contain calcium and phosphate ions and enzymes to degrade inhibitors of mineralization.[11] After bone formation the osteoblasts can become osteocytes as they are trapped within the bone or bone lining cells. However, the majority of osteoblasts undergo apoptosis at the end of bone formation. [1] Bone remodeling differs from modeling in that resorption and formation occur on the same bone surface during remodeling.

1.5 Bone Cells

Bone is comprised of three cell types: osteoblasts, osteocytes, and osteoclasts. The osteoblasts are responsible for building the bone matrix, while osteoclasts are responsible for breaking down bone matrix. Osteocytes are thought to be involved in signaling processes. Both osteoblasts and osteocytes come from the mesenchymal stem cell lineage, while the osteoclasts arise from hematopoietic stem cells. [12]

The commitment of mesenchymal stem cells to become osteoblasts is mediated by multiple factors, including Runx2, osterix, and Dlx5. [13] Bone morphogenic proteins are also inducers of osteoblast formation. These are members of the TGF-β superfamily and include BMP-2, BMP-4, and BMP-7. [14]

Osteocytes are the final stage of differentiation for osteoblasts. Osteocytes are located within lacunae in the bone matrix and have long extensions into the canaliculi, through which they communicate. Osteocytes produce large amounts of osteocalcin, galectin-3, and CD44. [14]

1.6 The Osteoclast

The osteoclast is responsible for bone resorption and, unlike osteoblasts and osteocytes, come from the monocyte/macrophage lineage. [15] Osteoclasts are developed in vitro with the addition of receptor activator of nuclear factor kappa-B ligand (RANKL) and macrophage colony-stimulating factor (M-CSF). [16, 17] Both proteins are produced by osteoblasts.

Osteoclasts resorb bone through the formation of a sealed environment between the cell and the underlying bone. This is accomplished using integrins, which are transmembrane receptors made of one α and one β subunit. [18] Specifically, the αvβ3 integrin is responsible for osteoclast-bone attachment. The αvβ3 binds to RGD motifs, found on various bone related protein, including bone sialoprotein and osteopontin. The αvβ3 integrin was discovered to be necessary for osteoclast attachment in a study using a

β3 integrin knock out mouse, which led to an increase in bone mass. [19] Inhibition of osteoclast binding through αvβ3 is a target under study for treatment of osteoporosis. [20]

The osteoclast requires a specialized cytoskeleton to function correctly. Binding to bone causes the osteoclast cytoskeleton to form two unique structures: the ruffled membrane and the sealing zone. The ruffled membrane gets its name from the shape created by the vesicles carrying cathepsin K, a lysosomal enzyme secreted by the osteoclast, and matrix metalloproteinases (MMPs) to the cell surface. [21] This area also houses proton pumps and a chloride ion channel used to bring the pH of this microenvironment to approximately 4.5 which dissolves bone's mineral component, leaving the organic component behind. [22] The organic matrix is primarily type 1 collagen, which is broken down by enzymes such as cathepsin K and tartrate-resistant acid phosphatase. The sealing zone is made from fibrillar actin and serves to separate the area being resorbed by the osteoclast from the surrounding environment. [23]

Osteoclast rearrangement is mediated through integrin signaling and the Rho family of small GTPases. Integrin signaling through the adaptor protein c-Src stimulates formation of the ruffled membrane [24]. Both Rho and Rac translocate to the cytoskeleton after binding GTP. Rho signalling leads to formation of the actin ring, [25, 26] while Rac signaling stimulates the formation of lamellipodia, which allows the osteoclast to migrate. [27]

1.7 Enzymes Involved in Bone Resorption

1.7.1 Cathepsin K (CTSK)

CTSK is an enzyme responsible for breaking down the organic matrix of bone. CTSK is primarily expressed by the osteoclast, with some expression occurring in the lung. [28] The gene for CTSK is found on chromosome 1 and transcription of CTSK is activated by RANKL and M-CSF. Transforming growth factor β1 (TGFβ1) and interleukin 10 (IL-10) both inhibit CTSK, which has a molecular mass of 24 kDa and consists of two domains, forming a v-shaped active site. [29]

1.7.2 Tartrate Resistant Acid Phosphatase (TRAP)

TRAP is a 35kDa metalloenzyme that breaks down phosphate esters or anhydrides. [30] While TRAP is primarily expressed in bone, it can also be found in the colon, kidney, liver, and testes. [28] TRAP has a molecular weight of about 35 kDa. Osteoclasts are commonly identified by staining for cells expressing TRAP.

1.8 Osteoclast Regulation

RANKL and M-CSF are the most well-known activators of osteoclastogenesis. RANKL is inhibited by Osteoprotegrin (OPG), a competitive inhibitor of RANKL. Both RANKL and OPG are produced by the osteoblast. [31] Interferon-γ (IFN-γ) also

suppresses osteoclast function [32] and vitamin D increases RANKL concentration while decreasing Osteoprotegrin levels, causing an increase in bone volume. [31]

The hormone estrogen prevents bone resorption and loss of estrogen in the aging process has been shown to contribute to bone loss. [33] Estrogen upregulates osteoblast formation through bone morphogenic protein 4 (BMP-4). [34] Glucocortocoids act as negative osteoclast regulators by increasing osteoblast apoptosis which leads to a decrease in RANKL. [35]

1.9 Bone Biomechanics

Bone can be strengthened in two ways: through the addition of more bone to help carry a load or through improving the bone's material composition. Bone strength can be quantified by various measurements, such as strain and stress. Strain is the change in length of an object divided by its original length and therefore has no unit. A strain can be tensile if the material is being stretched or compressive if the material is being pushed together. Shear stress is the angle of deformation by a force that is running parallel to the material, and is generated in bone during rapid changes in direction. Stress is a measure of force per unit area. [36]

Modulus is another measure of strength and is the slope of the initial linear part of the stress vs. strain curve **(**Figure 3**)**. This is also referred to as the elastic part of the curve since the removal of force allows the object being tested to return to its original state undamaged. The linear relationship of the stress-strain curve is also referred to as

Hooke's Law. The slope of the stress-strain curve in the elastic region is a measure of a material's stiffness. A larger slope of the stress-strain curve equals a higher stiffness. [36]

Two points of failure are observed when testing the strength of a material: yield failure and ultimate failure. Yield failure is the point where stress and strain do not have a linear relationship and is the point where permanent damage occurs. The region beyond this point on the stress-strain curve is referred to as the plastic region. Ultimate failure is the point at which the material being tested fails catastrophically. Toughness is a measure of a material's ability to resist fracture when put under a sudden load. [36]

1.10 Hyper-IgE Syndrome

Hyperimmunoglobulin E syndrome (HIES), also known as Job's syndrome, was originally discovered in 1966 by Davis et al. They described symptoms as a recurrent 'cold' and staphylococcal abscess. [37] HIES was and named in 1972 by Buckley at al. and characterized as having an increase in IgE concentration of up to 10 times the normal serum levels. [38]

HIES results in various infections and skeletal abnormalities as well as dental problems, including retained primary teeth and also failure of permanent teeth to erupt or permanent tooth eruption next to primary teeth, resulting in two rows of teeth. Eczema, skin abscesses, pneumonia, and candidiasis of the nail bed and mucus membranes are common. HIES patients also have an increased risk of bone fracture as shown in 1999 by Grimbacher et al. [39] Most fractures in the 30 patient study were a result of everyday

tasks, including diaper changing and line dancing The majority of these fractures were in long weight-bearing bones such as the femur along with the ribs and pelvis.

When fractures do occur, bacterial arthritis and osteomyelitis can be found. The study also found that scoliosis occurred in 76% of HIES patients. HIES can result in hyperextensible joints and a distinctive facial appearance, including an asymmetrical face, deep-set eyes, a broad nose, and a prominent forehead. [39, 40]

HIES is caused by one of two genetic mutations, autosomal-recessive HIES and autosomal-dominant HIES. [41] Both have been linked to chromosome 4. [42] A 2007 study by Holland et al. determined mutations of STAT3 was the cause of HIES. [43] All mutations were in either the DNA binding region or SH2 domain of STAT3.

1.11 Signal Transducers and Activators of Transcription

STAT3 is one of a family of 7 STAT proteins which includes Stat1, Stat2, Stat3, Stat4, Stat5a, Stat5b, and Stat6. The Stat proteins are part of the Janus kinase (JAK)-STAT signaling pathway. The JAK family of proteins includes JAK1, JAK2, JAK3, and Tyk2. [44] This pathway was originally discovered while looking at the actions of interferons. The STAT genes are located on multiple chromosomes: STAT1 and STAT4 are on chromosome 2, STAT3 STAT5a and STAT5b are located on chromosome 12, and STAT2 and STAT6 are on chromosome 17. All STATs are activated by phosphorylation of a tyrosine residue located around position 700. The STATs range in size between 750 and 850 amino acids long. [45]

1.12 JAK-STAT Pathway

The JAK-STAT pathway can be activated in many ways. Activation occurs with the binding of one of the interlukin-6 (IL-6) type cytokines to their receptors. This family of cytokines is also referred to as the gp130 family and consists of IL-6, IL-11, oncostatin M, leukemia inhibitory factor, cardiotrophin-1, and the novel neurotrophin-1/B-cell stimulatory factor-3. [46, 47] When these cytokines bind their respective receptors gp130 dimerizes, therefore activating JAK. Once JAK is activated it phosphorylates a tyrosine in a YXXQ motif of the receptor's cytoplasmic tail. The phosphorylated receptor then attracts the SH2 domain of a STAT, which then becomes phosphorylated at a tyrosine. This leads to the dimerization of the STAT and the movement of the dimerized STAT to the nucleus, where it can bind DNA and act as a transcription activator. [48] The JAK-STAT pathway can also be activated by STAT phosphorylation by epidermal growth factor (EGF) or platelet-derived growth factor (PDGF). In addition, JAKs may be activated by G-protein –coupled receptors **(**Figure 4**).** [49]

1.13 STAT3 Structure

STAT3 contains multiple domains, each with a different function. The N-domain, coiled-coil domain, linker domain, DNA binding domain, SH2 domain, and carboxy terminal transcriptional activation domain all make up the STAT3 protein. [50] (Figure 5)

The amino-terminal domain of STAT3 is involved in regulation. Two STAT3 dimers can bind to form a tetramer that helps form a more stable DNA binding complex. The amino-terminal domain may also be a drug target for anticancer drugs. [51, 52] The coiled-coil domain is a hydrophilic region made of four antiparallel α helices and is necessary for STAT3 to translocate to the nucleus. [53, 54] The coiled-coil region can also be used to bind the C-terminus of the interleukin-22 receptor to activate STAT3. Normally, STAT3 is activated by the association of the SH2 domain with a phosphorylated tyrosine on a cytokine receptor. [55] The coiled-coil region has also been found to be required for the STAT3 SH2 domain to bind a cytokine receptor through studies involving the deletion of α helixes 1 and 2. [56]

The DNA binding domain appears similar to an immunoglobulin, with two long β strands running perpendicular to the DNA. This domain consists of amino acids 320 to 480 and binds to interferon gamma activated sequences (GAS). [50]

The SH2 domain consists of two α helices surrounding an antiparallel β sheet. [53, 54] This region of STAT3 is responsible for both binding to receptors and dimer formation. The specificity of this region determines the differences in activation between members of the STAT protein family. [57]

1.14 STAT3 Activation

STAT3 can be activated in a number of ways. The primary method of activation is through the binding of IL-6 type cytokines to the extracellular part of their receptors to start the JAK-STAT pathway. Cytokines in this family include IL-6, IL-11, oncostatin M (OSM), leukemia inhibitory factor (LIF), ciliary neurotrophic factor (CNTF), and cardiotrophin-1 (CT-1). These cytokines are all similar in size and shape. The majority of IL-6 type cytokine receptors are transmembrane proteins with an extracellular amino end and one transmembrane domain. The one exception is the ciliary neurotrophic factor receptor, which uses a lipid anchored protein receptor. After ligand binding, the receptors dimerize. All cytokine signals use at least one gp130 as a receptor. IL-6 signaling uses two gp130s while all other cytokines use one gp130 and one leukemia inhibitory factor receptor. Oncostatin M uses one gp130 and one oncostatin M receptor. [46] All of these receptor subunits are capable of activating JAKs and recruiting STAT3. IL-6, IL-11, and CNTF all have their own α receptor subunits that are involved in the recruitment of the other two receptor subunits**. (**Figure 6**)** Dimerization of the two cytokine receptor subunits leads to activation of a janus kinase (JAK). The JAK trans-phosphorylates the cytoplasmic side of the receptor, which leads to recruitment of STAT3. JAKs phosphorylate a tyrosine residue of the YXXQ motif on the receptor.

STAT3 can also be activated by the receptors for epidermal growth factor (EGF), platelet derived growth factor (PDGF), or fibroblast growth factor (FGF), which are members of different receptor tyrosine kinases. These can phosphorylate STAT3 directly

without the use of a Janus kinase. Another method of activation for this pathway is the activation of Janus kinase through G-protein-coupled receptors. [58]

1.15 STAT3 Localization

The STAT proteins vary by the method in which they can enter the nucleus. [59] For example, STAT1 and STAT2 must be phosphorylated to enter the nucleus but STAT3 does not. An 11 amino acid long nuclear-localization signal of the coiled-coil domain is all that is required for STAT3 to enter the nucleus. [60] However, STAT3 must still be phosphorylated to bind DNA. The import of STAT3 to the nucleus is mediated by importin-α3, which binds to the nuclear-localization signal. [59]

1.16 Regulators of STAT3

There are various suppressors of STAT3 signalling. One group of proteins known to suppress all STATs is the suppressors of cytokine signaling (SOCS). SOCS can inhibit STAT3 signaling by interacting with the cytokine receptors, inhibiting JAKs, inhibiting the binding of STATs, and marking STATs for degradation by proteasomes. [61] SOCS were discovered by multiple groups, so they are also be referred to as JAK-binding protein (JAB) or STAT-induced STAT inhibitor (SSI). [58] Additionally, cytokine-inducible SH2-containing protein (CIS) is also a negative regulator of STAT3.

Inhibition and inactivation of STAT3 is carried out by protein inhibitor of activated STAT (PIAS). The family of PIAS includes PIAS1, PIAS3, PIASy, PIASxα/ARIP3, and PIASxβ /Miz1. PIAS3 is regulates STAT3 by binding phosphporylated STAT3 and preventing DNA binding. [62] Cyclin D1 is also an important negative regulator of STAT3 and is overexpressed in various forms of cancer. [63, 64]

1.17 STAT3 Knockout Mouse Model

The knockout of STAT3 is lethal at the embryonic stage and STAT3 knockout mouse embryos usually do not survive beyond 7.5 days. STAT3 is the only member of the STAT protein family in which knockout leads to death of the animal. Therefore, to study STAT3, a conditional knockout model is necessary. This is accomplished using the Cre-loxp recombination system.

1.18 STAT3 in Bone

STAT3 is known to play a major role in bone homeostasis. Osteoblast-specific STAT3 knockout mice are decreased in size and bone density. These mice also display decreased bone mineral density and bone area. Bone growth rate and strength are decreased. [65] The osteoblast-specific STAT3 knockout also shows a decrease in load-driven bone formation and an increase in reactive oxygen species (ROS) levels, indicating decreased mitochondrial activity. [65]

In vitro studies revealed that inhibition of JAK2 with AG490 causes decreased osteoclastogenesis. An osteoclast precursor cell line treated with AG490 resulted in decreased cell proliferation, regardless of how much RANKL was added. This demonstrated that the JAK2/STAT3 pathway is involved in RANKL mediated osteoclastogenesis. [66]

1.19 Research Goals

We hypothesize that the loss of STAT3 in osteoclasts will lead to decreased osteoclast proliferation and therefore an increase in bone size and strength. To test this, we acquired two osteoclast-specific STAT3 knockout mouse models and observed bone mineral density, bone structure, strength, and conducted histomorphometrical analysis of the mouse's femur at 8 and 16 weeks. Osteoclasts were also isolated to determine their activity levels.

CHAPTER 2. MATERIALS AND METHOD

2.1 Conditional STAT3 Knockout Mice

Osteoclast-specific mice were generated using the Cre-loxP system. Floxed STAT3 mice were bred with mice expressing Cre recombinase. In this experiment, two mouse strains were used: one in which Cre is driven by the promoter for cathepsin K (CTSK) and another driven by the tartrate-resistant acid phosphatase (TRAP) promoter. The Stat3 floxed mice were obtained from Dr.Xin-Yuan Fu in the Department of Microbiology and Immunology, Indiana University School of Medicine. Both the CTSK- Cre and TRAP-Cre mice came from the University of Melbourne, Australia. The STAT3 floxed mice contain two loxp sequences flanking exons 18-20 of the STAT3 gene. Mice that were homozygous for the loxP sites ($STAT3^{flox/flox}$) and the Cre transgene (CTSK-cre or TRAP-cre) were used as conditional knockout mice. Mice that were wild-type for the loxP site ($STAT3^{+/+}$) and homozygous for the Cre transgene were used for control. All procedures were performed in accordance with guidelines provided by the IACUC.

2.2 PCR for STAT3 and Cre Genes

Mouse genotype was confirmed through polymerase chain reaction (PCR). Approximately 2mm was cut from the tip of the tail of each mouse and stored in a 1.5mL microcentrifuge tube. Scissors were sterilized between mice using 70% ethanol. A lysis buffer was prepared with 50mM Tris, 50mM KCl, 2.5mM EDTA, 0.4% NP-40, and 0.45% Tween-40. 0.4mg/mL proteinase K was added immediately before use. 100µL of the lysis buffer was added to each tube. The tubes with tail samples were placed in a 56°C water bath overnight. The next day the tubes were transferred to a 95°C dry bath for 10 min. The tail samples were then diluted with 100µL autoclaved milliQ water. 1µL of this lysate was transferred to a PCR tube with 12.5µL REDTaq® ReadyMix™, 5.5µL water, 0.5µL (0.5µM) forward primer, and 0.5µL reverse primer. Primer sequences are: Stat3 forward 5'-ATT GGA ACC TGG GAC CAA GTG G-3', Stat3 reverse 5'-ACA TGT ACT TAC AGG GTG TGT GC-3', Cre forward 5'-GAG TGA TGA GGT TCG CAA GA-3', Cre reverse 5'-CTA CAC CAG AGA CGG AAA TC-3'. The PCR tubes were put in a PTC-11 Peltier Thermal Cycler for 39 cycles (1 min at 94°C, 30 sec at 94°C, 30 sec at 55°C, and 30 sec at 68°C). The tubes were then removed and loaded into a 2.5% agarose gel with 1x SYBR safe DNA stain. A 100 bp ladder was used. After electrophoresis, there are bands of three different sizes. The STAT3 $^{flox/flox}$ mice have two loxp sequences and produces a 520bp band. STAT3$^{+/+}$ mice lack the loxp sequences and therefore produce a smaller490bp band. Cre mice produce a 615bp band if it is present (Figure 7). STAT3$^{flox/flox}$, Cre^{+} mice will be referred to as conditional knockout (KO) and STAT3$^{+/+}$, Cre^{+} mice will be referred to as wild type (WT).

2.3 Immunohistochemistry

Slides of paraffin-embedded mouse femur and tibia were deparaffinized using three changes of xylene for 5 minutes each and then rehydrated in graded ethanols. The slides were transferred to phosphate buffered saline (PBS) for 5 minutes before being immersed in DeCal Epitope retrieval Solution for 30 minutes. All slides spent two 5 minute sessions in methanol and two in PBS to rinse the DeCal solution. Slides were transferred to a PBS+ 0.3% Triton X-100 solution for 10 minutes and stored in PBS until use.

Next, a 3% H_2O_2/methanol solution was applied for 5 minutes and then rinsed twice with PBS. A 1.5% goat serum blocking solution (VectaStain ABC kit) was applied to each slide for 30 minutes. After rinsing in PBS, a STAT3 primary antibody solution was applied to each slide before storing overnight at 4°C.

The following day, all primary antibody solution was rinsed from the slides using PBS before a biotinylated secondary antibody (VectaStain ABC kit) was applied to all slides with the exception of the negative control, which received 1.5% goat serum blocking solution for 45 minutes.

After two rinses with PBS an avidin-conjugated peroxidase (ACP) solution was applied to the slides for 30 minutes. The negative control received a 1.5% goat serum blocking solution. Finally, the ACP solution was rinsed away with PBS and a peroxidase substrate solution was applied to all slides for 1 minute.

2.4 Bone Mineral Density (PIXImus)

Bone mineral density (BMD) and bone mineral content (BMC) were observed in femurs and lumbar vertebra 4 (L4) from 8 and 16 week old mice using a PIXImus densitometer. Bones were placed in the center of the scanning tray. BMD and BMC were calculated using the PIXImus program.

2.5 Mechanical Testing

The left femur from mice euthanized at 8 weeks old was extracted and stored in saline at -20°C prior to 3-point bending. All femurs were loaded into a 500lb. actuator (Test Resources) with a 25 lb. loading cell. The span of the bottom 2 contacts was set at 6mm apart to accommodate all femurs while the top contact was placed midway between these points. The midpoint of each femur was placed at the top contact. Load was applied in a posterior-anterior direction by the top contact at 0.03mm per second until failure or 30N. Force-displacement and stress-strain curves were generated during this time. Break points were found by measuring from the distal end to the break point at the anterior face of each femur. [67]

2.6 Micro CT

Left femurs were isolated from mice euthanized at 8 and 16 weeks old and stored in saline at -20°C. Femurs were scanned using a Skyscan 1172 micro-CT scanner (Bruker-microCT, Belgium). All images were acquired with a 6.0μm pixel size. Data were analyzed using the program CTan and 3D models were constructed using CTvol.

2.7 Osteoclast Cell Culture

Femur and tibia for both right and left legs were collected for each mouse. Soft tissue was removed from the bones and the bones were placed in αMEM containing 10% FBS and antibiotics for transport. Bones were then transferred in αMEM supplemented with 2% FCS and more soft tissue was removed. After cleaning, the bones were moved to a petri dish containing 10% FCS in αMEM. The epiphyses were cut from each bone and the marrow was flushed from the diaphyses into a centrifuge tube using a syringe and needle with 10% FCS in αMEM. Cells were washed twice before use. Cells were counted on a hemacytometer.

Next, 0.2μL/mL M-CSF and 0.5μL/mL RANKL (R&D Systems) were added to each tube. The cell suspension was then dispensed into the wells of a Corning Osteoassay culture plate (Corning Incorporated), starting with the smallest wells and working up to the larger ones. The 96 well plate received 200μL/well (100,000 cells). 1mL per well (500,000 cells) was dispensed into the 24 well plate and 2mL/well

(1,000,000 cells) was added to the 6 well plates. The cells were fixed with 2.5% glutaraldehyde in phosphate buffered saline and stained for TRAP before counting.

2.8 Histology

Specimens were fixed in formalin for at least 24 hours and dehydrated using a series of ethanols before being cleared using xylenes. All specimens were infiltrated using unpolymerized methyl methacrylate and unpolymerized methyl methacrylate with 4% dibutyl phthalate. Specimens were transferred to methyl methacrylate, 3% dibutyl phthalate, and 0.25 % Perkadox 16. Polymerization occurred at room temperature. Thin sections of trabecular bone were cut 4-10 μm thick using a rotary microtome and mounted on microscope slides. Thick sections of cortical bone were cut 100μm thick using a diamond-wire saw and sanded to a final thickness of 30μm before observation.

2.8.1 Tartrate Resistant Acid Phosphatase (TRAP) Stain

Sections were first deplastified in acetone and rehydrated using ethanols. Slides containing the sections were then incubated in a pH 5.0 sodium acetate buffer containing 0.2M sodium acetate and 50mM sodium tartrate dibasic dihydrate for 20 min. Slides were then transferred to a pH 5.0 sodium acetate buffer containing 0.2M sodium acetate, 50mM sodium tartrate dibasic dihydrate, 0.5mg/mL napthol AS-MX phosphate, and 1.1 mg/mL fast red TR salt for 1 hour at 37°C. Sections were then counterstained with hematoxylin. [68]

2.8.2 VKM Stain

Sections were deplastified and rehydrated as above. Slides were then stained in a 5% silver nitrate solution, rinsed, and stained in a sodium carbonate-formaldehyde solution containing 5 % sodium carbonate and 25mL formaldehyde per 100mL. Slides were then rinsed twice and transferred to Farmer's diminisher for 20 seconds. After washing, sections were stained in a 2% MacNeal's tetrachrome solution for 20 min. Sections were rinsed 3 times, dehydrated in ethanol, and cleared using xylenes. [69]

2.9 Histomorphometry

All mice were injected with the fluorescent dyes calcein and alizarin. Calcein was injected one week before sacrifice and alizarin was injected 2 days before sacrifice. Sections were observed using an Olympus BX53 light/fluorescent microscope and Olympus DP72 camera interfaced with Osteomeasure™ software version 1.01(OsteoMetrics Inc, Decatur GA). An area 0.4mm proximal from the growth plate and 0.5mm medial from cortical bone (approx. 1.4mm^2 for labels and Trap stain, 0.60mm^2 was examined for VKM slides). All measurements were taken at 200x for labels and Trap stain, 400x for VKM stain. All measurements and abbreviations were made according to Parfitt et al. [70] These abbreviations and formulas used can also be found in Tables 1 and 2. Mice lacking one of the fluorescent labels were given a mineral appositional rate of 0.1μm/day to avoid leaving a MAR of zero and allow for calculation of bone formation rates. [71]

2.10 Statistics

Data were reported as mean ± standard deviation. Difference between group means was tested using a 2-sample t-test in Minitab (Minitab Inc. PA). Statistical significance was assumed if $P < 0.05$.

CHAPTER 3. RESULTS

3.1 Verification of Osteoclast Specific Knockout Mice

Mice were generated as described previously described. An immunohistochemical stain was performed to verify the knockout of STAT3 in osteoclasts. The expression of STAT3 was shown to be decreased in osteoclast specific STAT3 KO mice (Figure 9).

3.2 Comparison of Mouse Body Weight and Femur Length

There were no significant differences in mouse body weight (Figure 10) or femur length (Figure 11) among TRAP-Cre or CTSK-Cre mice. Both males and females were similar at age 8 weeks and 16 weeks. Unless otherwise noted, data was collected for 12 WT female and male mice and for 17 cKO females and males.

3.3 CTSK Specific Knockout Female Mice Decrease in BMD

At 8 weeks, CTSK specific Stat3 knockout female mice demonstrated an 8.6 % significant decrease in BMD ($p < 0.05$) and a 13.6% decrease in BMC ($p < 0.05$) of the left femur compared to control (Figure 12). BMD values were 0.0431±0.003g/cm^2 for female WT and 0.0394 ±0.003 for g/cm^2 for female cKO mice. WT female BMC was 0.0162±0.003g and cKO was 0.014±0.002g. Males showed a non-significant 1.1% decrease in BMD (WT 0.0463±0.004g/cm^2, cKO 0.0458±0.007 g/cm^2) and a 3.7% decrease in BMC in Stat3 KO mice compared to their littermate controls (WT 0.0188±0.002g, cKO 0.0181±0.004g). However, at 16 weeks the BMD and BMC of Stat3 knockout females decreased 2.0% and 4.8% respectively (BMD: WT-0.0494±0.002 g/cm^2 cKO-0.0485±0.004 g/cm^2; BMC WT-0.0208±0.001g cKO-0.0208±0.003g) which was not a significant difference. Neither BMD nor BMC changed in the 16 week old CTSK specific Stat3 knockout males as compared to littermate controls (Figure 13). The TRAP specific Stat3 KO mice demonstrated no changes in BMD or BMC in the males or females that were 8 weeks of age (Figure 14).

3.4 CTSK Specific KO Mice Trabecular Bone at 8 Weeks Old

CTSK specific Stat3 KO mice had significantly decreased trabecular bone volume and trabecular number at 8 weeks of age in males and females. Trabecular separation was significantly increased in CTSK specific STAT3 KO mice compared to controls (Figure 15). Bone volume/tissue volume (BV/TV) was significantly (42%) in CTSK

specific Stat3 KO females compared to controls, while males displayed a significant 25% decrease in BV/TV. Specifically, female WT BV/TV was 9.26±2.3% and cKO BV/TV was 5.37±1.3%, while male WT BV/TV was 14.85±3.8% and cKO was 11.13±3.5%). Trabecular separation showed significant increases of 22% and 23% among CTSK specific Stat3 KO females and males, respectively. Trabecular number significantly decreased 40% in female Stat3 KO mice (WT- 0.0745±0.0166/μm and cKO- 0.045±0.013/μm) and 31% in males. These differences can be observed in the 3 dimensional models in Figure 15. On the other hand, no significant differences were detected between the 8 week old TRAP specific Stat3 KO and control with respect to BV/TV, trabecular thickness, trabecular number, or separation.

3.5 CTSK Specific KO Mice Trabecular Bone 16 Week of Age

At 16 weeks of age, the CTSK specific Stat3 KO mice had significantly higher trabecular bone than did controls (Figure 16). Specifically, BV/TV increased 46% among the female Stat3 KO mice compared to controls while BV/TV increased 13% in males. The trabecular number was also significantly higher in Stat3 KO compared to controls (45% in females and 13% in males). Trabecular separation was significantly elevated in Stat3 KO females (18%), but a 5% increase was observed in male Stat3 KO mice compared to controls. There were no significant differences detected in trabecular thickness among males or females.

3.6 CTSK Specific KO Increases the Number of Osteoclasts

Data gathered from a TRAP stain of the distal femur revealed a significant decrease in osteoclast number among CTSK specific Stat3 KO mice compared to controls (Figure 17). The osteoclast number was significantly reduced 36% in female CTSK specific Stat3 KO (WT-71±23, cKO 45.6±32) and was reduced 9% (not statistically significant) in CTSK specific Stat3 KO males (WT-71.7±23, cKO- 64.8±24) compared to age and gender matched controls. Although the trend for a reduction in the male KO mice, the standard deviation values were too high to detect a significant difference. Calculation of osteoclast number/tissue area reveals similar results. The osteoclast surface/bone surface was significantly lower (50%) in female CTSK specific Stat3 KO mice compared to controls (WT-1.24±0.5mm, cKO-0.63±0.4mm). The TRAP specific cKO mice had a 41% decrease in osteoclast number/bone surface in females (WT-10.9±1.6/mm, cKO 6.3±2.7/mm) and a 30 % reduction in males (WT-9.4±2.16/mm, cKO-6.5±2.04/mm) (see Figure 18).

3.7 CTSK Specific STAT3 KO Trabecular BFR at 8 Weeks Old

Analysis of calcein and alizarin labeled bone surfaces showed that the bone formation rate of CTSK specific Stat3 KO females was significantly lower (28%) than that observed in WT controls (WT-356±54 $\mu m^3/\mu m^2$/year, cKO 256±163 $\mu m^3/\mu m^2$/year (Figure 19). The mineralizing surface/bone surface was also significantly decreased by 20% in Stat3 KO females compared to WT controls (WT-42.0±7.69%, cKO-

33.6±9.80%). The Stat3 KO males displayed a 14% increase in mineral apposion rate and a 5% decrease in mineralizing surface/bone surface; however, the standard deviation on these values was too high to detect a significant difference likely owing to the fact that a few mice had only one fluorescent label present. No significant differences were detected with respect to osteoblast number or osteoid surface.

3.8 Cortical Bone Size and Growth Rate in STAT3 KO Mice

Average cross-sectional bone area and cortical thickness were found not to be different in cortical bone at the midshaft in both 8 and 16 week old mice. Analysis of the labeled femur midshaft showed that there are minimal decreases in periosteal MS/BS of STAT KO females and endocortical MAR in Stat3 KO males at age 8 weeks (Figure 21). No differences were found in cortical bone area or growth rates of TRAP specific STAT3 KO mice.

3.9 Mechanical Testing: 3 Point Bending

Femurs from 8 week old CTSK specific Stat3 KO and wild-type mice were subjected to 3 point bending to determine their strength. As shown in Figure 22, although not significantly different, the female Stat3 KO femurs had a 20% decrease in total toughness (WT-20.2±4.94MJ/m^3, cKO-16.1±5.53 MJ/m^3). Similarly, although not statistically significant, Stat3 KO male femurs had a 19% increase in stiffness (WT-58.0±9.51N/mm, cKO-71.8±20.6N/mm). The ultimate force required to break the femur

increased by 13% in Stat3 KO males compared to their WT controls (WT-12.4N±1.7, cKO-14.3±3.1N). Of note, total work was significantly decreased 23% in Stat3 KO female femurs compared to WT controls (WT-11.2±2.7mJ, cKO-8.63±2.7mJ. All other measurements were similar.

3.10 Osteoclast Cell Culture

Osteoclasts were cultured from 6 week old female CTSK specific STAT3 KO and WT mice. There was no significant difference detected in osteoclast number (Figure 23). Resorption area decreased in STAT3 KO mouse cultures compared to WT, although the difference was not statistically significant. Two mice were gathered for each group. Triplicate wells were prepared from each mouse and two mice were utilized from each group (CTSK specific STAT3 KO and WT controls).

CHAPTER 4. DISCUSSION

4.1 Decreased Osteoclast Number in STAT3 KO

Recent studies have tied STAT3 to the osteoclast. STAT3 has been shown to be involved in RANKL mediated osteoclast differentiation. A study by Li et al. used the JAK2 inhibitor AG490 and found that osteoclast differentiation was decreased without JAK-STAT signaling. [66] An experiment using siRNA was also performed to knockdown STAT3. They found that some RANKL induced genes were downregulated and others were not. This shows that STAT3 is important for osteoclastogenesis but it is not the only transcription factor required for RANKL mediated osteoclastogenesis. [66]

4.2 Osteoclast Number and BV/TV in Trabecular Bone

The decreased osteoclast number and trabecular bone volume in 8 week old mice suggests communication from the osteoclast to the osteoblast (Figure 15 and 17). While no major differences were observed in bone formation rates on the fluorescent- labeled distal femur or from the osteoblast cell count, the osteoclast is known to have some influences on osteoblast activity.

Osteoblast-osteoclast communication through RANKL and OPG is much better understood than osteoclast-osteoblast communication. Candidates for osteoclast-osteoblast communication include platelet derived growth factor, EphB4-EphrinB2 interactions, and even osteoclast precursors. Ephrin signaling through Eph can cause both osteoblast production and inhibition of osteoclastogenesis depending on the direction of signal. Ephrin B2 binding EphB4 leads to increased osteoblast differentiation, while EphB4 binding to Ephrin B2causes a decrease in osteoclastogenesis. [72] Immune system cells have also been tied to signaling the osteoblast. Monocytes have been shown to bring an increase in osteoblast differentiation. This study also found that STAT3 signaling was responsible for osteoblast differentiation, highlighting the role of STAT3 in osteoblasts as well as osteoclasts. [73]

4.3 Differences in Bone Phenotypes at age 8 and 16 Weeks

The phenotypes of CTSK specific STAT3 KO mice reversed between the ages of 8 and 16 weeks. In the 8 week old mice, trabecular bone volume and number was decreased among STAT3 KO (Figure 15). In the 16 week old group, the STAT3 KO mice had a larger trabecular bone volume and number (Figure 16). Although the difference observed in bone phenotype between 8 week old and 16 week old mice may suggest changes with aging/development, caution must be taken in this interpolation as different control mice were used in the 8 week vs. 16 week studies.

Specifically, each genotype of the control mice in the 8 week old study was $STAT3^{+/+}$ Cre+, while the genotype of the 16 week old control mice was $STAT3^{flox/flox}$ Cre-. The latter mice came from a previous study.

Some of our findings also implicate gender-based differences. For example, female CTSK specific STAT3 KO mice had larger decreases in osteoclast number and trabecular bone volume than did the males. This suggests sex hormones, such as estrogen, may have influences on bone through STAT3.

4.4 Males Exhibit Stronger Cortical Bone In STAT3 KO

As seen in Figure 22**,** although not significantly different from controls, the CTSK specific STAT3 KO males displayed similar or elevated bone mechanical parameters compared to their wild-type controls without any differences in cortical thickness or bone area at 8 weeks of age. These observations are of interest as the female CTSK specific STAT3 KO femurs had reduced biomechanical properties with total work being significantly reduced compared to WT female femurs. This suggests that STAT3 may also have a gender-based effect on the quality of bone matrix.

4.5 Future Plans

Future plans for this experiment include looking into the mechanism by which STAT3 decreased osteoclast number and trabecular bone parameters. Observing histological slides for the 16 week old CTSK and TRAP specific STAT3 KO mice would

be beneficial. Mechanical testing of these same groups should also be done. Generating 16 week old CTSK control mice with the same genotype used as a control in all other experiments will also be done to confirm findings.

LIST OF REFERENCES

LIST OF REFERENCES

1. Dempster, D.W., *Anatomy and functions of the adult skeleton*, in *Primer on the metabolic bone diseases and disorders of mineral metabolism*. 2006, The American Society for Bone and Mineral Research: Washington DC. p. 7-11.
2. Brodsky, B. and. Persikov A.V, *Molecular structure of the collagen triple helix.* Advances in Protein Chemistry, 2005. **70**: p. 301-39.
3. Seibel, M.J., *Biochemical markers of bone remodeling.* The Journal of Clinical Endocrinology and Metabolism North Am, 2003. **32**(1): p. 83-113, vi-vii.
4. Gokhale JA, R., Boskey AL, *The biochemistry of bone*, in *Osteoporosis*, F.D. Marcus R, Kelsey J, Editor. 2001, Academic Press: San Diego CA. p. 107-188.
5. Glimcher, M., *The nature of the mineral phase in bone: Biological and clinical implications*, in *Metabolic Bone Disease and Clinically Related Disorders*, S.K. LV Avioli, Editor. 1998, Academic Press: San Diego, CA. p. 23-51.
6. Landis, W.J., *The strength of a calcified tissue depends in part on the molecular structure and organization of its constituent mineral crystals in their organic matrix.* Bone, 1995. **16**(5): p. 533-44.
7. Eppell, S.J., et al., *Shape and size of isolated bone mineralites measured using atomic force microscopy.* Journal of Orthopedic Research, 2001. **19**(6): p. 1027-34.
8. Haapasalo, H., et al., *Exercise-induced bone gain is due to enlargement in bone size without a change in volumetric bone density: a peripheral quantitative computed tomography study of the upper arms of male tennis players.* Bone, 2000. **27**(3): p. 351-7.
9. Parfitt, A.M., *Physiologic and pathogenetic significance of bone histomorphometric data*, in *Disorders of Bone Miner Metabolism*, M.F. FL coe, Editor. 2002, Lippincott, Williams, and Wilkins: Baltimore, MD. p. 469-485.
10. Roodman, G.D., *Cell biology of the osteoclast.* Experimental Hematology, 1999. **27**(8): p. 1229-41.
11. Anderson, H.C., *Matrix vesicles and calcification.* Current Rheumatology Reports, 2003. **5**(3): p. 222-6.
12. Aubin, J.E., and Stein, G. S., *Bone formation: maturation and functional activities of osteoblast lineage cells*, in *Primer on the metabolic bone diseases and disorders of mineral metabolism.* 2006, The American Society for Bone and Mineral Research: Washington DC. p. 20-29.
13. Gaur, T., et al., *Canonical WNT signaling promotes osteogenesis by directly stimulating Runx2 gene expression.* Journal of Biological Chemistry, 2005. **280**(39): p. 33132-40.

14. ten Dijke, P., et al., *Signal transduction of bone morphogenetic proteins in osteoblast differentiation.* Journal of Bone and Joint Surgery Am, 2003. **85-A Suppl 3**: p. 34-8.
15. Suda, T., et al., *Modulation of osteoclast differentiation and function by the new members of the tumor necrosis factor receptor and ligand families.* Endocrine Reviews, 1999. **20**(3): p. 345-57.
16. Boyle, W.J., W.S. Simonet, and D.L. Lacey, *Osteoclast differentiation and activation.* Nature, 2003. **423**(6937): p. 337-42.
17. Pixley, F.J. and E.R. Stanley, *CSF-1 regulation of the wandering macrophage: complexity in action.* Trends in Cell Biology, 2004. **14**(11): p. 628-38.
18. Hynes, R.O., *Integrins: bidirectional, allosteric signaling machines.* Cell, 2002. **110**(6): p. 673-87.
19. Ross, F.P. and S.L. Teitelbaum, *alphavbeta3 and macrophage colony-stimulating factor: partners in osteoclast biology.* Immunological Review, 2005. **208**: p. 88-105.
20. Teitelbaum, S.L., *Osteoporosis and integrins.* The Journal of Clinical Endocrinology and Metabolism, 2005. **90**(4): p. 2466-8.
21. Teitelbaum, S.L., Abu-Amer Y., and. Ross F.P, *Molecular mechanisms of bone resorption.* Journal of Cellular Biochemistry, 1995. **59**(1): p. 1-10.
22. Teitelbaum, S.L. and Ross F.P., *Genetic regulation of osteoclast development and function.* Nature Reviews Genetics, 2003. **4**(8): p. 638-49.
23. Vaananen, H.K., et al., *The cell biology of osteoclast function.* Journal of Cell Science, 2000. **113 (Pt 3)**: p. 377-81.
24. Horne, W.C., et al., *The role(s) of Src kinase and Cbl proteins in the regulation of osteoclast differentiation and function.* Immunological Reviews, 2005. **208**: p. 106-25.
25. Jaffe, A.B. and Hall A., *Rho GTPases: biochemistry and biology.* The Annual Review of Cell and Developmental Biology, 2005. **21**: p. 247-69.
26. Chellaiah, M.A., *Regulation of actin ring formation by rho GTPases in osteoclasts.* Journal of Biological Chemistry, 2005. **280**(38): p. 32930-43.
27. Fukuda, A., et al., *Regulation of osteoclast apoptosis and motility by small GTPase binding protein Rac1.* Journal of Bone and Mineral Research, 2005. **20**(12): p. 2245-53.
28. Chiu W.S.M., J.F.M., Notini A.J., Cassady A.I.,. Zajac J.D, and. Davey R.A, *Transgenic Mice That Express Cre Recombinase in Osteoclasts.* genesis, 2004. **39**: p. 178-185.
29. Lecaille, F., D. Bromme, and Lalmanach G., *Biochemical properties and regulation of cathepsin K activity.* Biochimie, 2008. **90**(2): p. 208-26.
30. Oddie, G.W., et al., *Structure, function, and regulation of tartrate-resistant acid phosphatase.* Bone, 2000. **27**(5): p. 575-84.
31. Kostenuik, P.J. and Shalhoub V., *Osteoprotegerin: a physiological and pharmacological inhibitor of bone resorption.* Current Pharmaceutical Design, 2001. **7**(8): p. 613-35.
32. Takayanagi, H., *Mechanistic insight into osteoclast differentiation in osteoimmunology.* Journal of Molecular Medecine (Berl), 2005. **83**(3): p. 170-9.

33. Syed, F. and Khosla S., *Mechanisms of sex steroid effects on bone.* Biochemical and Biophysical Research Communications, 2005. **328**(3): p. 688-96.
34. Matsumoto, Y., et al., *Estrogen facilitates osteoblast differentiation by upregulating bone morphogenetic protein-4 signaling.* Steroids, 2013. **78**(5): p. 513-20.
35. Weinstein, R.S., et al., *Promotion of osteoclast survival and antagonism of bisphosphonate-induced osteoclast apoptosis by glucocorticoids.* Journal of Clinical Investigation, 2002. **109**(8): p. 1041-8.
36. Rubin, C.R.a.J., *Biomechanics and Mechanobiology of Bone*, in *Primer on the metabolic bone diseases and disorders of mineral metabolism*. 2006, The American Society for Bone and Mineral Research: Washington DC. p. 36-42.
37. Davis, S.D., Schaller J., and Wedgwood R.J, *Job's Syndrome. Recurrent, "cold", staphylococcal abscesses.* Lancet, 1966. **1**(7445): p. 1013-5.
38. Buckley, R.H., Wray B.B., and Belmaker E.Z., *Extreme hyperimmunoglobulinemia E and undue susceptibility to infection.* Pediatrics, 1972. **49**(1): p. 59-70.
39. Grimbacher, B., et al., *Hyper-IgE syndrome with recurrent infections--an autosomal dominant multisystem disorder.* New England Journal of Medecine, 1999. **340**(9): p. 692-702.
40. AF Freeman, S.H., *The hyper-IgE syndromes.* Immunology and Allergy Clinics of North America, 2008. **2**: p. 277-291.
41. He, J., et al., *STAT3 mutations correlated with hyper-IgE syndrome lead to blockage of IL-6/STAT3 signalling pathway.* Journal of Biosciences, 2012. **37**(2): p. 243-57.
42. Grimbacher, B., et al., *Genetic linkage of hyper-IgE syndrome to chromosome 4.* American Journal of Human Genetics, 1999. **65**(3): p. 735-44.
43. Holland, S.M., et al., *STAT3 mutations in the hyper-IgE syndrome.* New England Journal of Medecine, 2007. **357**(16): p. 1608-19.
44. Akira, S., *Functional roles of STAT family proteins: lessons from knockout mice.* Stem Cells, 1999. **17**(3): p. 138-46.
45. Darnell, J.E., Jr., *STATs and gene regulation.* Science, 1997. **277**(5332): p. 1630-5.
46. Heinrich, P.C., et al., *Interleukin-6-type cytokine signalling through the gp130/Jak/STAT pathway.* Biochemical Journal, 1998. **334 (Pt 2)**: p. 297-314.
47. Senaldi, G., et al., *Novel neurotrophin-1/B cell-stimulating factor-3: a cytokine of the IL-6 family.* Proceedings of the National Acadamy of Science U S A, 1999. **96**(20): p. 11458-63.
48. Ishihara, K. and Hirano T., *Molecular basis of the cell specificity of cytokine action.* Biochimica and Biophysica Acta, 2002. **1592**(3): p. 281-96.
49. Ihle, J.N., *STATs: signal transducers and activators of transcription.* Cell, 1996. **84**(3): p. 331-4.
50. Husby, J., et al., *Molecular dynamics studies of the STAT3 homodimer:DNA complex: relationships between STAT3 mutations and protein-DNA recognition.* Journal of Chemical Information and Modeling, 2012. **52**(5): p. 1179-92.

51. Timofeeva, O.A., et al., *Rationally designed inhibitors identify STAT3 N-domain as a promising anticancer drug target.* ACS Chem Biol, 2007. **2**(12): p. 799-809.
52. Zhang, X. and Darnell, J.E Jr., *Functional importance of Stat3 tetramerization in activation of the alpha 2-macroglobulin gene.* Journal of Biological Chemistry, 2001. **276**(36): p. 33576-81.
53. Ma, J., et al., *A novel sequence in the coiled-coil domain of Stat3 essential for its nuclear translocation.* Journal of Biological Chemistry, 2003. **278**(31): p. 29252-60.
54. Chen, X., et al., *Crystal structure of a tyrosine phosphorylated STAT-1 dimer bound to DNA.* Cell, 1998. **93**(5): p. 827-39.
55. Dumoutier, L., et al., *New activation modus of STAT3: a tyrosine-less region of the interleukin-22 receptor recruits STAT3 by interacting with its coiled-coil domain.* Journal of Biological Chemistry, 2009. **284**(39): p. 26377-84.
56. Zhang, T., et al., *The coiled-coil domain of Stat3 is essential for its SH2 domain-mediated receptor binding and subsequent activation induced by epidermal growth factor and interleukin-6.* Molecular and Cellular Biology, 2000. **20**(19): p. 7132-9.
57. Hemmann, U., et al., *Differential activation of acute phase response factor/Stat3 and Stat1 via the cytoplasmic domain of the interleukin 6 signal transducer gp130. II. Src homology SH2 domains define the specificity of stat factor activation.* Journal of Biological Chemistry, 1996. **271**(22): p. 12999-3007.
58. Lim, C.P. and Cao X, *Structure, function, and regulation of STAT proteins.* Molecular Biosystems, 2006. **2**(11): p. 536-50.
59. Reich, N.C. and Liu L., *Tracking STAT nuclear traffic.* Nature Reviews Immunology, 2006. **6**(8): p. 602-12.
60. Liu, L., McBride K.M., and Reich N.C., *STAT3 nuclear import is independent of tyrosine phosphorylation and mediated by importin-alpha3.* Proceedings of the National Academy of Science U S A, 2005. **102**(23): p. 8150-5.
61. Ortiz-Munoz, G., et al., *Suppressors of cytokine signaling modulate JAK/STAT-mediated cell responses during atherosclerosis.* Arteriosclerosis Thrombosis and Vascular Biology, 2009. **29**(4): p. 525-31.
62. Liu B, S.K., *The PIAS protein family and Tc-PTP*, in *Signal Transducers and Activators of Transcription (STATs): Activation and Biology*, L.D. Sehgal DE, Hirano T, Editor. 2003, Kluwer Academic Publishers: The Netherlands. p. 75-85.
63. Alle, K.M., et al., *Cyclin D1 protein is overexpressed in hyperplasia and intraductal carcinoma of the breast.* Clinical Cancer Research, 1998. **4**(4): p. 847-54.
64. Wang, T.C., et al., *Mammary hyperplasia and carcinoma in MMTV-cyclin D1 transgenic mice.* Nature, 1994. **369**(6482): p. 669-71.
65. Zhou, H., et al., *Osteoblast/osteocyte-specific inactivation of Stat3 decreases load-driven bone formation and accumulates reactive oxygen species.* Bone, 2011. **49**(3): p. 404-11.
66. Li, G.H., et al., *AG490 inhibits NFATc1 expression and STAT3 activation during RANKL induced osteoclastogenesis.* Biochemical and Biophysical Research Communications, 2013.

67. Wallace, J.M., et al., *Inbred strain-specific effects of exercise in wild type and biglycan deficient mice.* Annals of Biomedical Engineering, 2010. **38**(4): p. 1607-17.
68. Erlebacher, A. and Derynck R., *Increased expression of TGF-beta 2 in osteoblasts results in an osteoporosis-like phenotype.* Journal of Cellular Biology, 1996. **132**(1-2): p. 195-210.
69. Schenk, R., Olah ,AJ and Herrmann, W, *Preparation of calcified tissue for light microscopy*, in *Methods of Calcified Tissue Preparation*, G. Dickson, Editor. 1984, Elsevier: New York. p. 1-56.
70. Parfitt, A.M., et al., *Bone histomorphometry: standardization of nomenclature, symbols, and units. Report of the ASBMR Histomorphometry Nomenclature Committee.* Journal of Bone and Mineral Research, 1987. **2**(6): p. 595-610.
71. Bivi, N., et al., *Cell autonomous requirement of connexin 43 for osteocyte survival: consequences for endocortical resorption and periosteal bone formation.* Journal of Bone and Mineral Research, 2012. **27**(2): p. 374-89.
72. Zhao, C., et al., *Bidirectional ephrinB2-EphB4 signaling controls bone homeostasis.* Cell Metabolism, 2006. **4**(2): p. 111-21.
73. Nicolaidou, V., et al., *Monocytes induce STAT3 activation in human mesenchymal stem cells to promote osteoblast formation.* PLoS One, 2012. **7**(7): p. e39871.

TABLES

Table 1 Abbreviations and formulas for parameters used in cortical bone

parameter	**abbreviation**	**units**	**formula**
cortical bone area	Ct.B.Ar	mm2	
cortical tissue area	Ct.T.Ar	mm2	
cortical marrow area	Ct.Ma.Ar	mm2	
bone volume/tissue volume	Ct.BV/TV	%	Ct.B.Ar/Ct.T.Ar
cortical thickness	Ct.Th	um	
periosteal perimeter	Ps.Pm	mm	
periosteal inter-label thickness	Ps.Ir.L.Th	um	
periosteal single-label surface/bone surface	Ps.sL.S/BS	%	
periosteal double-label surface/bone surface	Ps.dL.S/BS	%	
periosteal mineralizing surface/bone surface	Ps.MS/BS	%	Ps.(dL.Pm+sL.Pm/2)Ps.B.Pm
periosteal mineral apposition rate	Ps.MAR	um/d	Ps.Ir.L.Th/time between labeling
periosteal bone formation rate/bone surface	Ps.BFR/BS	$um^3/um^2/y$	Ps.MAR*(Ps.MS/BS)*365
periosteal bone formation rate/bone volume	Ps.BFR/BV	%/y	Ps.MAR*(Ps.(dL.Pm+sL.Pm/2)/Ct.B.Ar)*365
periosteal bone formation rate/tissue volume	Ps.BFR/TV	%/y	Ps.MAR*(Ps.(dL.Pm+sL.Pm/2)/Ct.T.Ar)*365
endocortical perimeter	Ec.Pm	mm	
endocortical inter-label thickness	Ec.Ir.L.Th	um	
endocortical single-label surface/bone surface	Ec.sL.S/BS	%	
endocortical double-label surface/bone surface	Ec.dL.S/BS	%	
endocortical mineralizing surface/bone surface	Ec.MS/BS	%	Ec.(dL.Pm+sL.Pm/2)Ec.B.Pm
endocortical mineral apposition rate	Ec.MAR	um/d	Ec.Ir.L.Th/time between labeling
endocortical bone formation rate/bone surface	Ec.BFR/BS	$um^3/um^2/y$	Ec.MAR*(Ec.MS/BS)
endocortical bone formation rate/bone volume	Ec.BFR/BV	%/y	Ec.MAR*(Ec.(dL.Pm+sL.Pm/2)/Ct.B.Ar)*365
endocortical bone formation rate/tissue volume	Ec.BFR/TV	%/y	Ec.MAR*(Ec.(dL.Pm+sL.Pm/2)/Ct.T.Ar)*365

Table 2 Abbreviations and formulas for parameters used in trabecular bone

parameter	abbreviation	units	formula
tissue area	T.Ar	mm^2	
bone area	B.Ar	mm^2	
bone perimeter	B.Pm	mm	
double-label perimeter	dL.Pm	mm	
single-label perimeter	sL.Pm	mm	
inter-label thickness	Ir.L.Th	um	
mineralizing surface/bone surface	MS/BS	%	(dLPm+sLPm/2)B.Pm
mineral apposition rate	MAR	um/day	Ir.L.Th/time between labeling
bone formation rate/bone surface	BFR/BS	$um^3/um^2/y$	MAR*(MS/BS)
bone formation rate/bone volume	BFR/BV	%/y	MAR*((dL.Pm+sL.Pm/2)/B.Ar)*365
bone formation rate/tissue volume	BFR/TV	%/y	MAR*((dL.Pm+sL.Pm/2)/T.Ar)*365
bone volume/tissue volume	BV/TV	%	B.Ar/T.Ar
osteoclast perimeter	Oc.Pm	mm	
number of osteoclasts	N.Oc	#	
osteoclast surface/bone surface	Oc.S/BS	%	Oc.Pm/B.Pm
number of osteoclasts/tissue area	N.Oc/T.Ar	$\#/mm^2$	N.Oc./T.Ar
number of osteoclasts/bone perimeter	N.Oc/B.Pm	#/mm	N.Oc/B.Pm
number of osteoclasts/osteoclast perimeter	N.Oc/Oc.Pm	#/mm	N.Oc/Oc.Pm
osteiod area	O.Ar	mm^2	
osteoblast perimeter	Ob.Pm	mm	
number of osteoblasts	N.Ob	#	
osteiod volume/tissue volume	OV/TV	%	O.Ar/T.Ar
osteoid volume/bone volume	OV/BV	%	O.Ar/B.Ar
osteoid surface/bone surface	OS/BS	%	O.Ar/B.Pm
osteoblast surface/bone surface	Ob.S/BS	%	Ob.S/B.Pm
number of osteoblasts/bone perimeter	N.Ob/B.Pm	#/mm	N.Ob/B.Pm
number of osteoblasts/osteoblast perimeter	N.Ob/Ob.Pm	#/mm	N.Ob/Ob.Pm

FIGURES

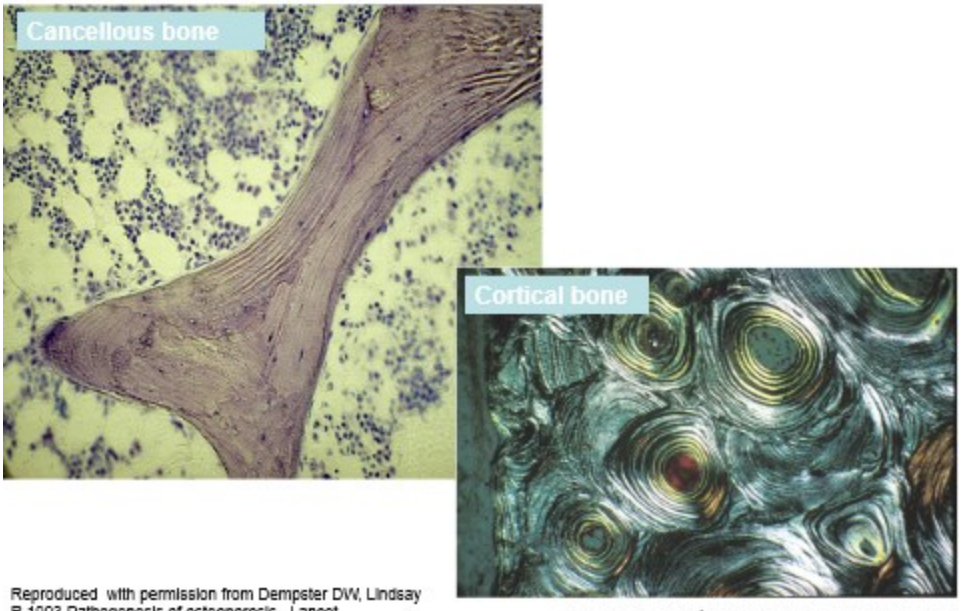

Figure 1: Osteons. Osteons of trabecular bone (left) and cortical bone (right) [1]

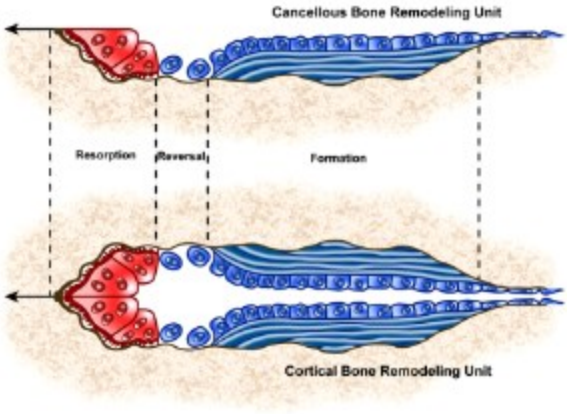

Figure 2: Bone remodeling units. Bone remodeling units for trabecular bone (top) and cortical bone (bottom) [1]

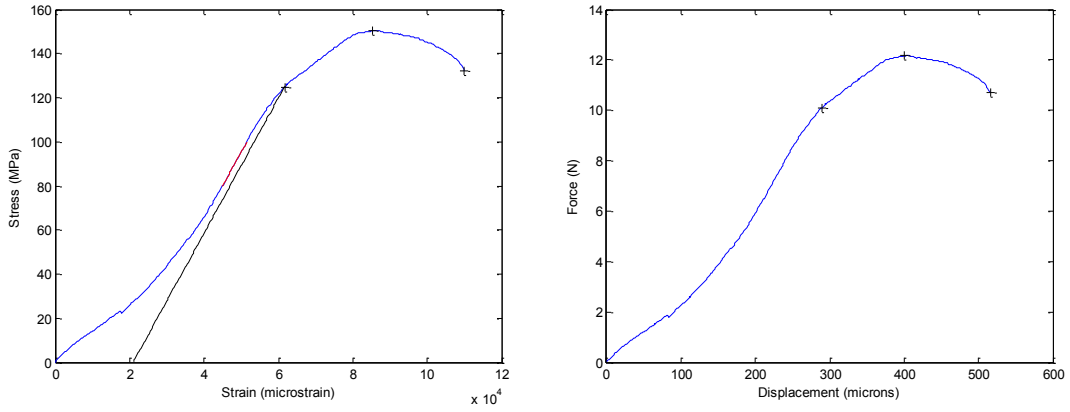

Figure 3: Stress-stain curve (left) and force-displacement curve (right)

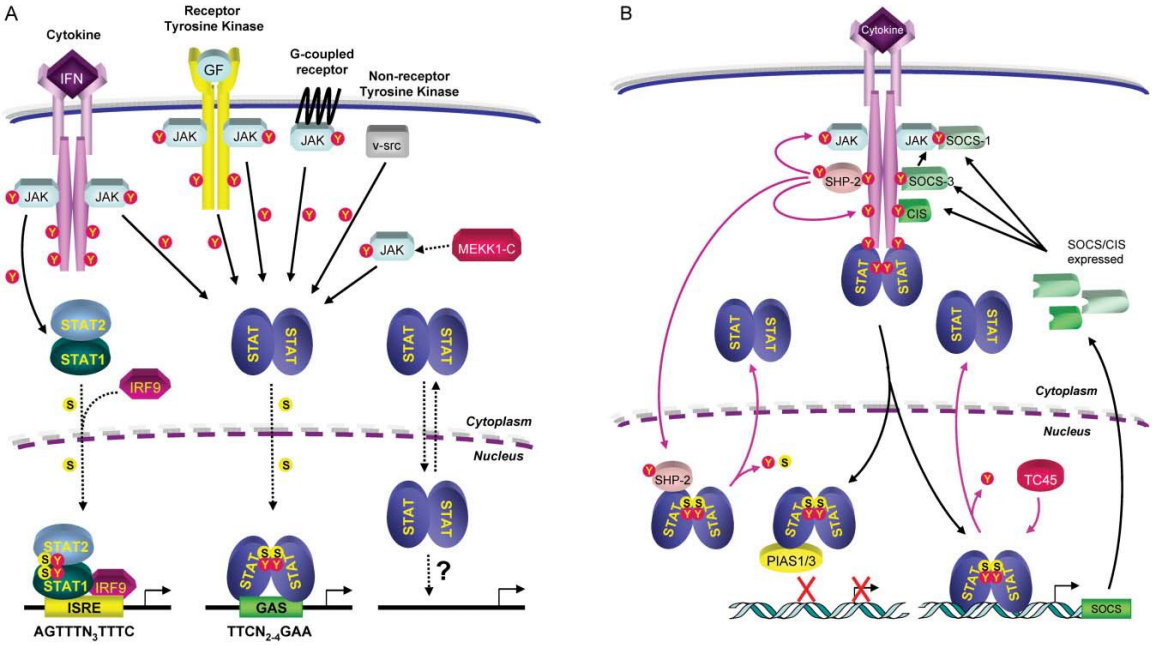

Figure 4: STAT3 activation. STAT3 is activated through the JAK-STAT signaling pathway along with other starting points [58]

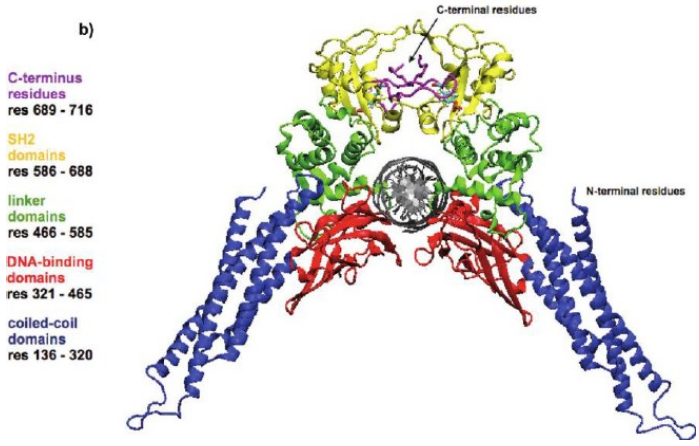

Figure 5: STAT3 crystalline structure [50]

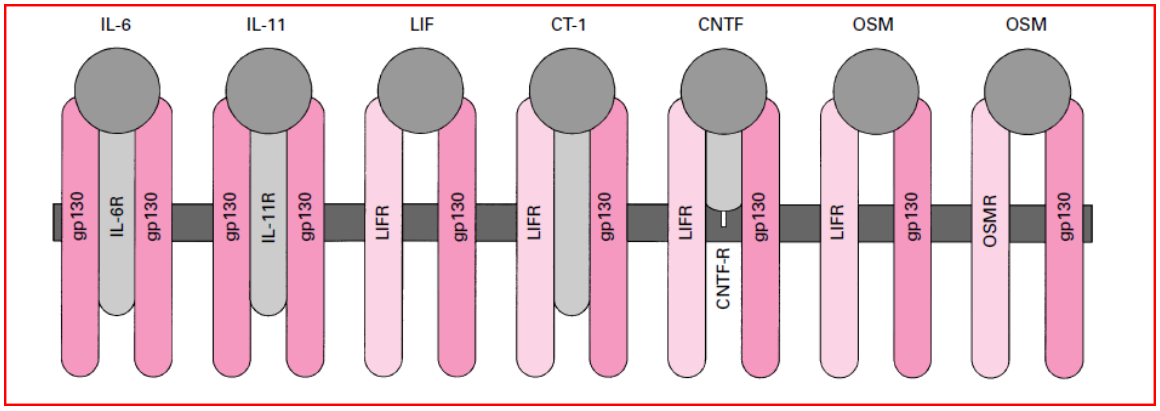

Figure 6: Membrane receptors for IL-6 family cytokines [46]

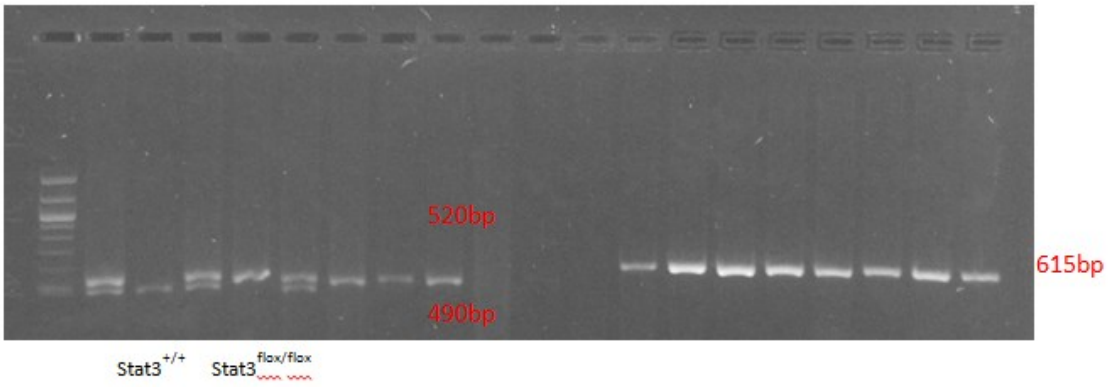

Figure 7: Determination of mouse genotype. The smaller 490bp belongs to the $STAT3^{+/+}$ (wilt type) mice while the 520bp fragments contain loxp sites. The 615 bp band represents Cre.

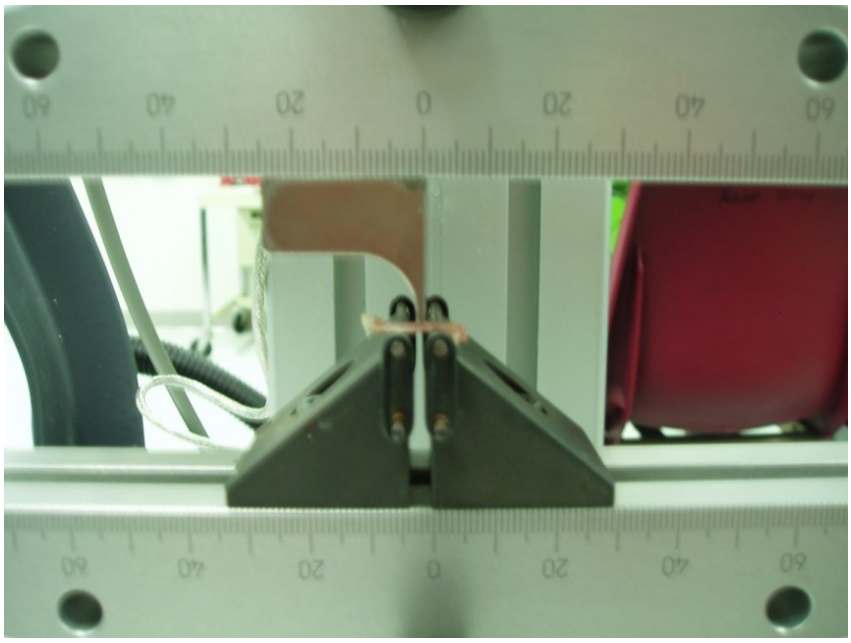

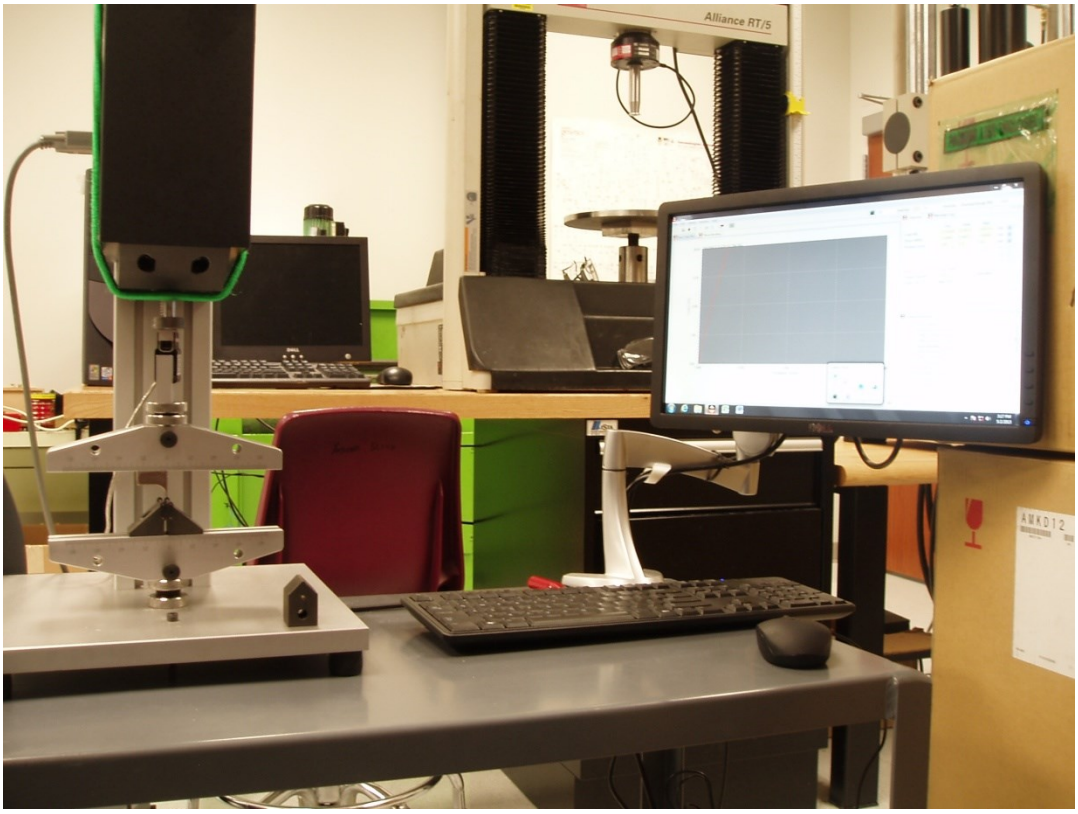

Figure 8: Mechanical testing: bone loaded into position for three point bending (top) and actuator (bottom)

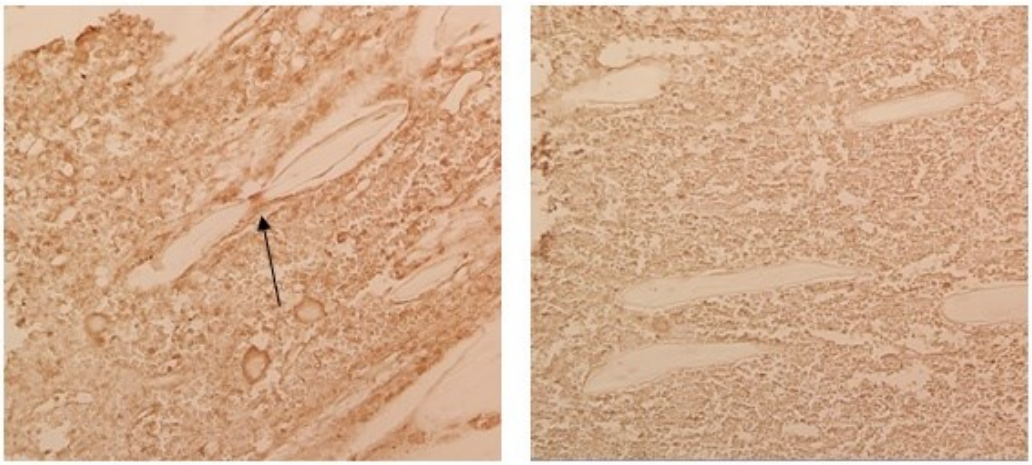

A B

Figure 9: Immunohistochemical staining. Decalcified mouse femurs were stained using an anti-phosphorylated STAT3 primary antibody; A is a wild-type mouse while B is an 8 week old CTSK specific STAT3 KO. The arrow is pointing to a phospho-STAT3 positive osteoclast

A)

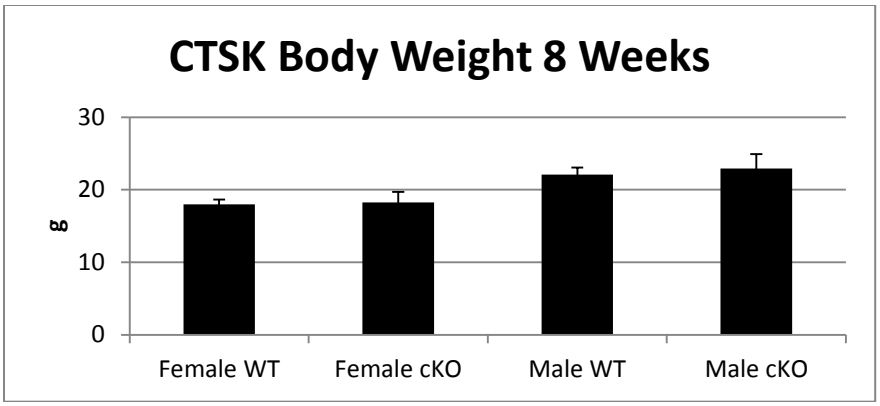

B)

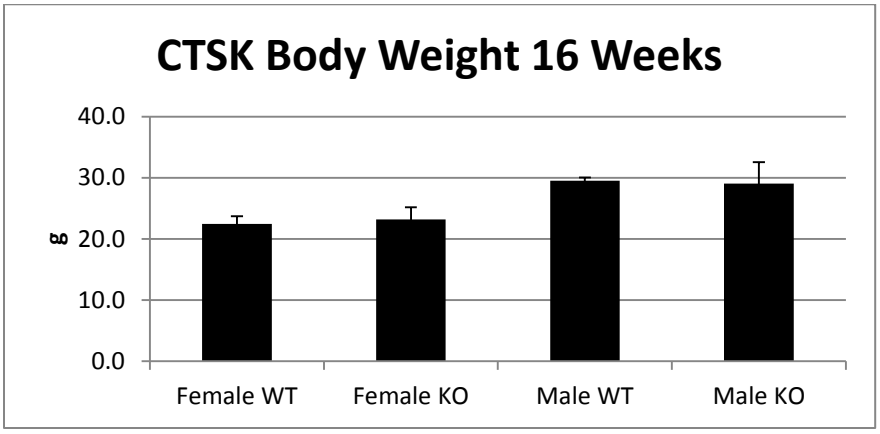

C)

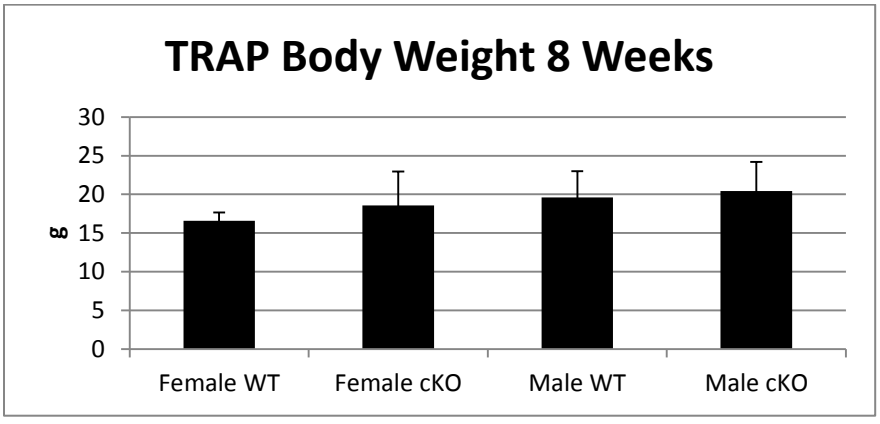

Figure 10: Body weights of osteoclast specific Stat3 mice at age 8 and 16 weeks (A=CTSK 8 week, B=CTSK 16 week, C=TRAP 8 week). No significant differences were detected

A)

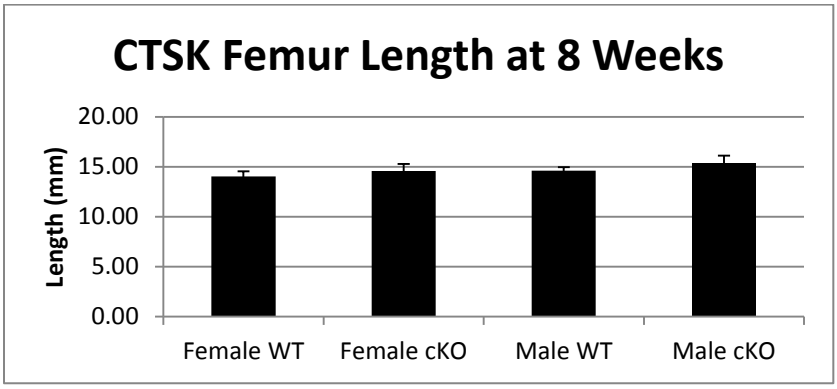

B)

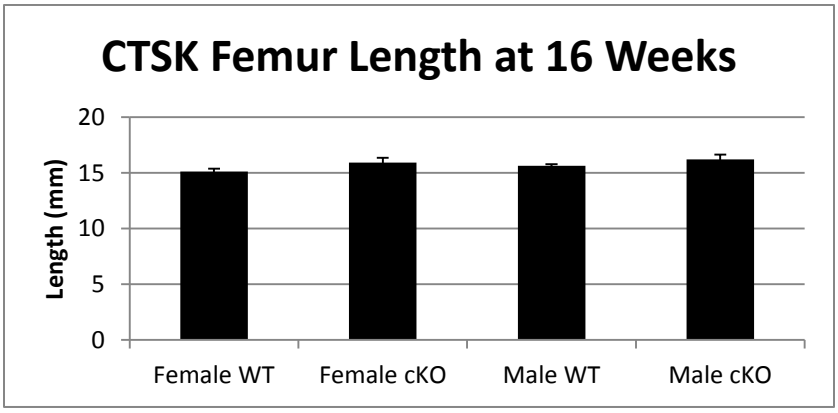

C)

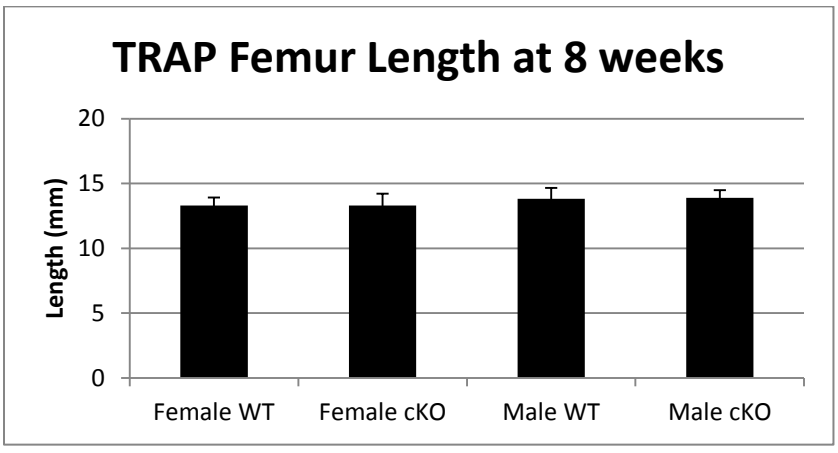

Figure 11: Femur length of osteoclast specific STAT3 KO mice at age 8 and 16 weeks (A= CTSK 8 weeks, B=CTSK 16 weeks, C=TRAP Femur 8 weeks). No differences were detected.

A)

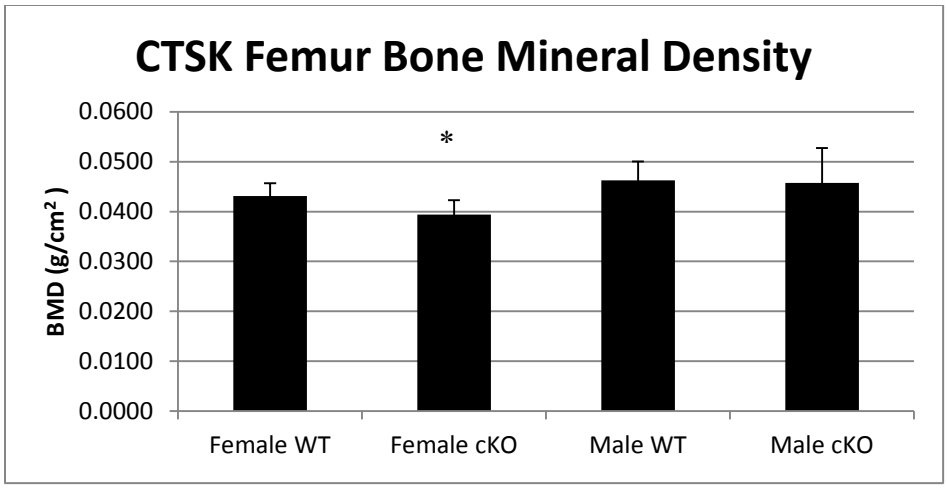

B)

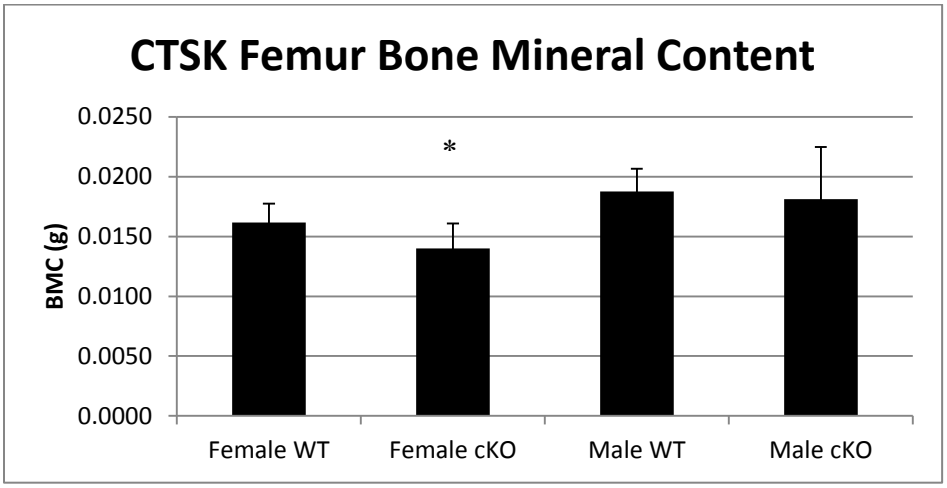

Figure 12: BMD and BMC of 8 week CTSK STAT3 KO mice. Bone mineral density (A) and bone mineral content (B) of CTSK STAT3 KO mice. Left femurs were collected from mice at 8 weeks of age and scanned using a PIXImus scanner. Bone mineral density and bone mineral content were decreased in female cKO mice compared to female WT mice (*: $p<0.05$)

A)

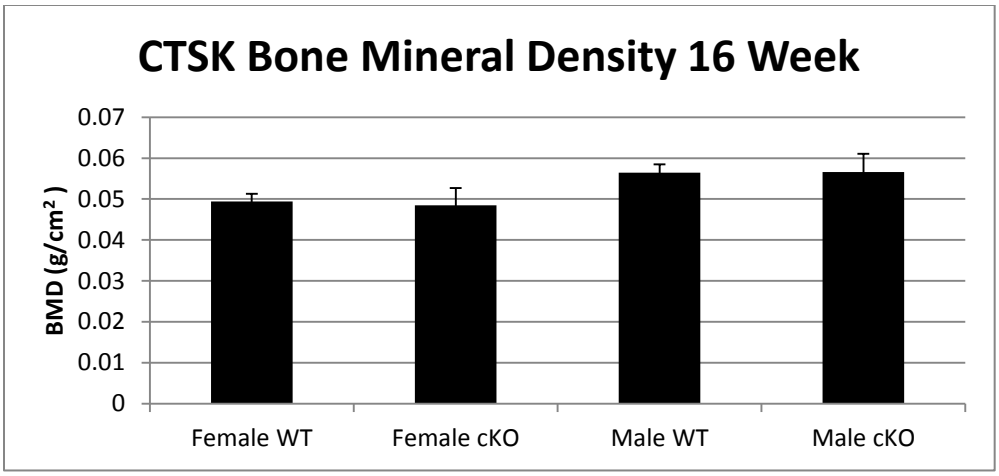

B)

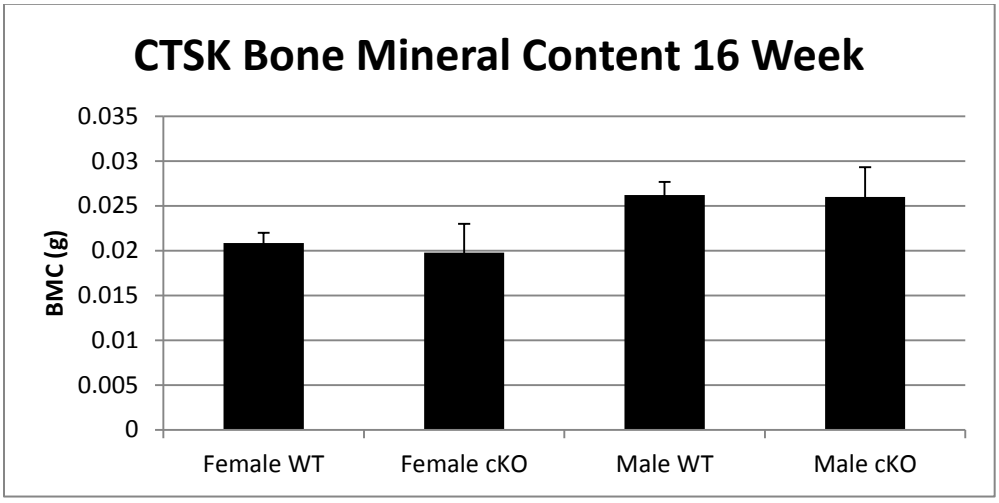

Figure 13: BMD and BMC of adult CTSK mice. Bone mineral density (A) and bone mineral content (B) of femurs from adult CTSK mice. Left femurs were collected from mice at 16 weeks of age and scanned using a PIXImus scanner. No significant differences were detected.

A)

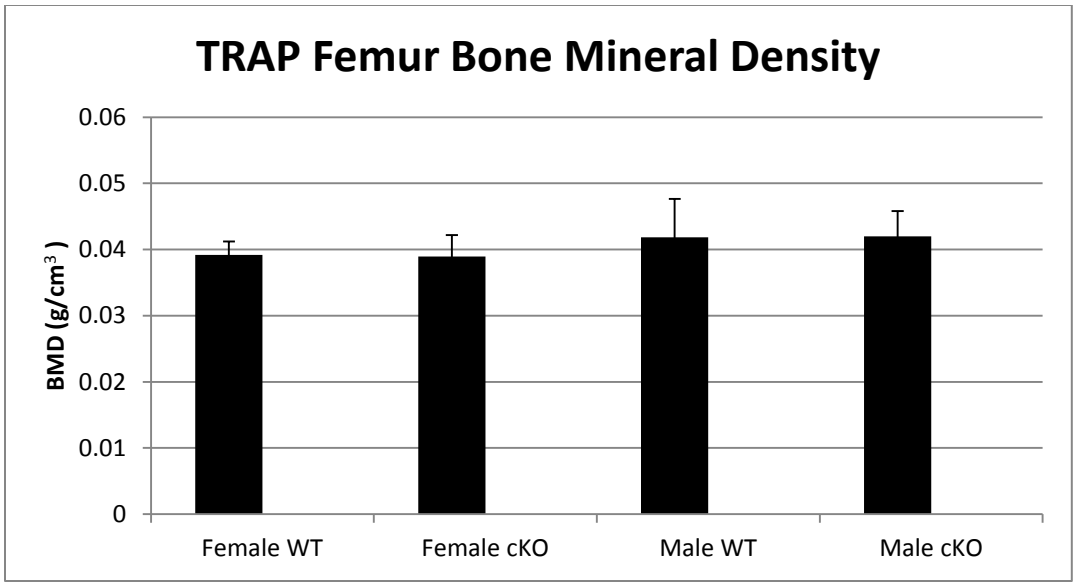

B)

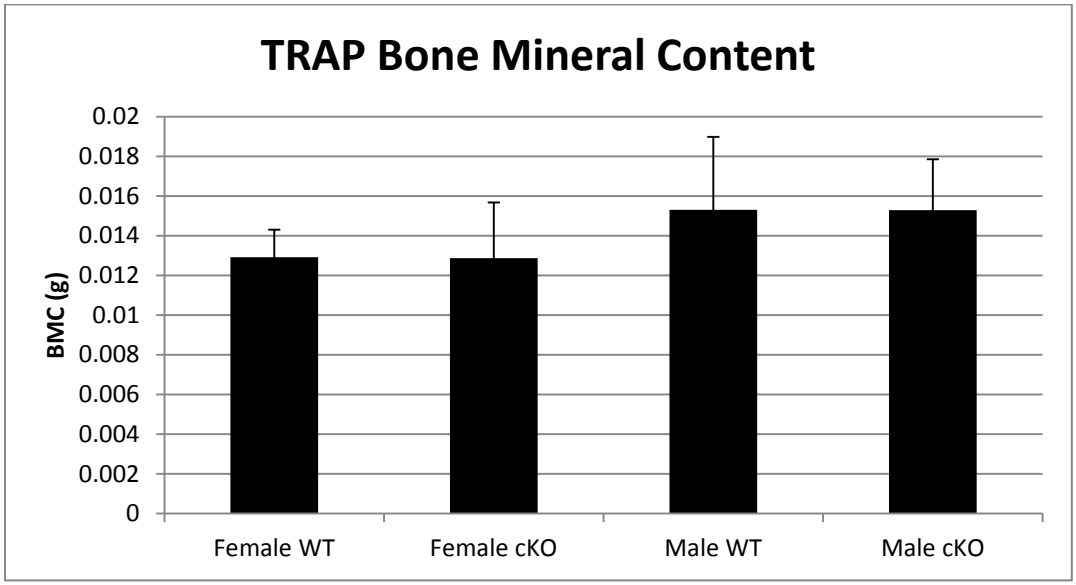

Figure 14: BMD and BMC of 8 week old TRAP STAT3 KO mice. Bone mineral density (top) and bone mineral content (bottom) of femurs from 8 week old TRAP STAT3 KO mice. Left femurs were collected from mice and scanned using a PIXImus scanner. No significant differences were detected.

A)

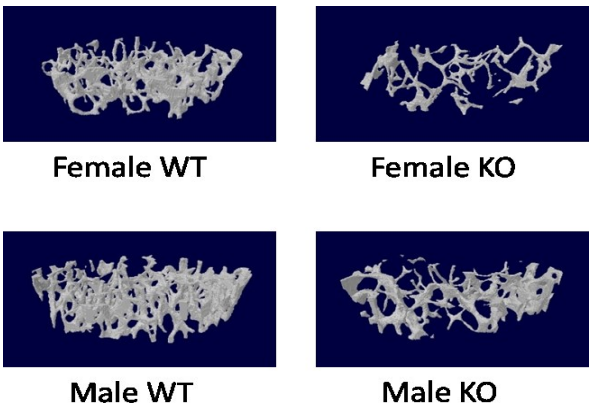

B)

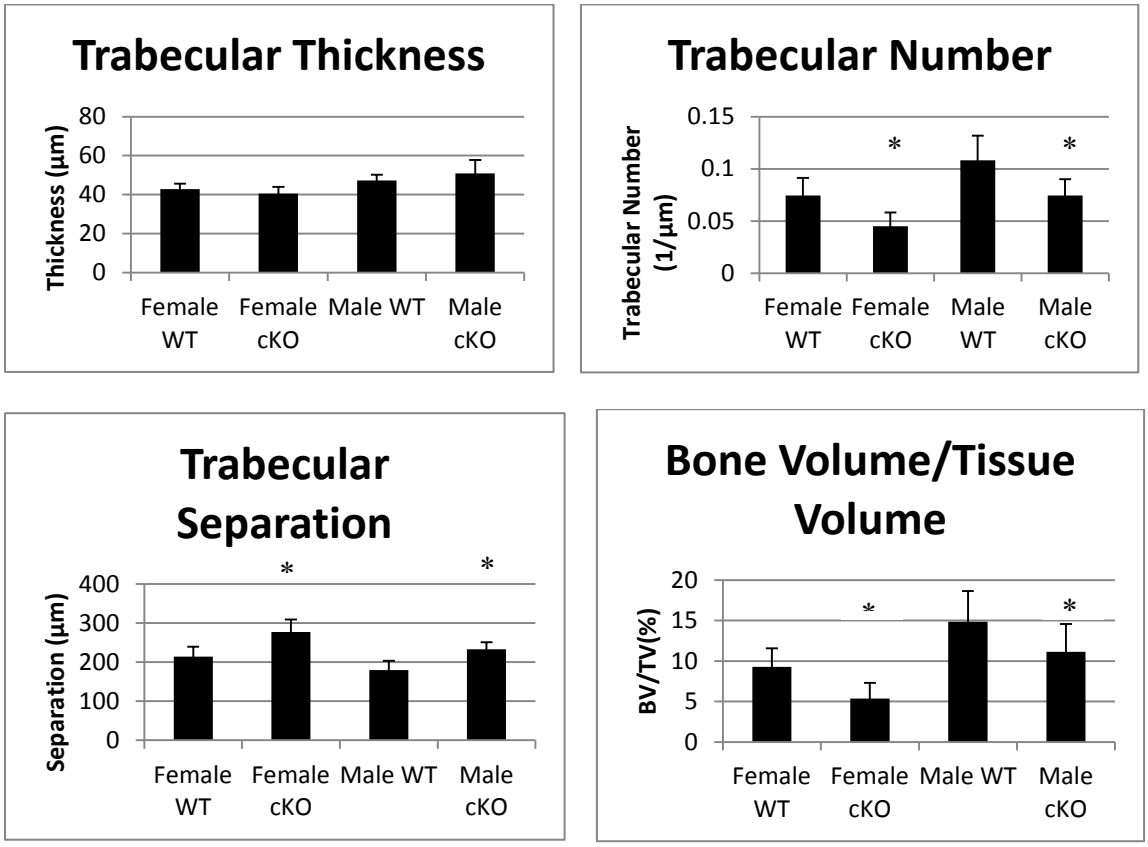

Figure 15: Trabecular bone structure of 8 week old CTSK mice. Three dimensional models of a 0.5mm thick trabecular bone area 1mm proximal from growth plate (A) and graphs depicting data gathered from the same area (B) Data were collected from microCT scan of left femurs. Trabecular number and Bone volume/tissue volume significantly increased in cKO males and females compared to age and gender matched controls, while trabecular separation was significantly lower in cKO female mice compared to WT females (*: $p < 0.05$).

A)

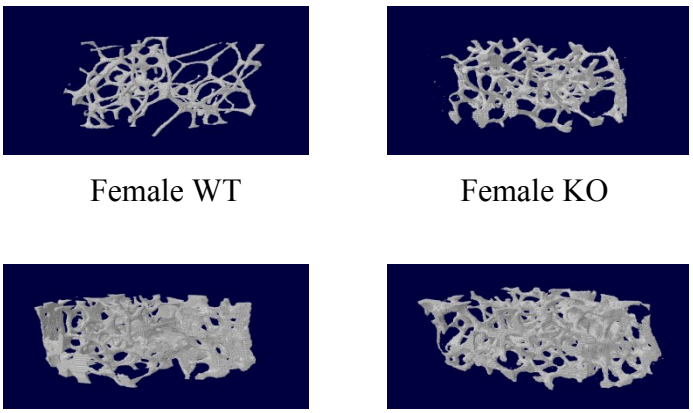

Female WT Female KO

Male WT Male KO

B)

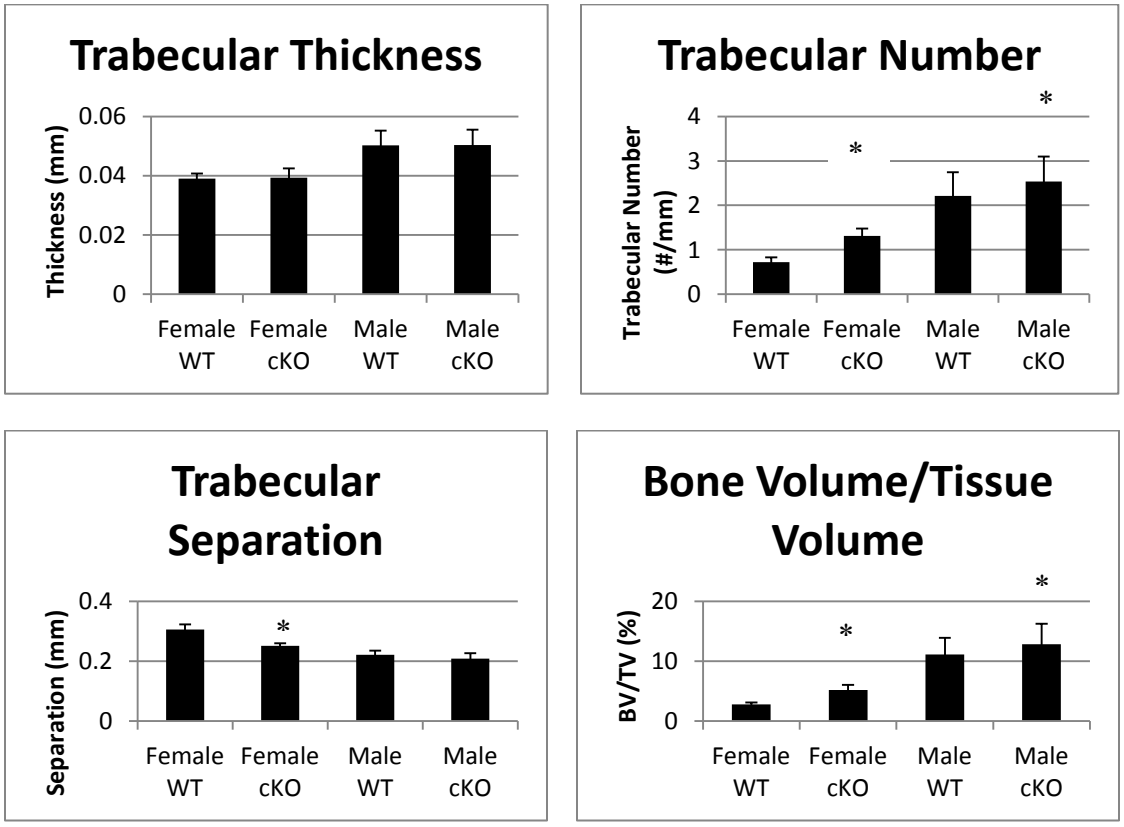

Figure 16: Trabecular bone structure of 16 week old CTSK mice. Three dimensional models of a 1mm thick trabecular bone area 1mm proximal from growth plate (A) and graphs depicting data gathered from the same area (B) Data were collected from microCT scan of left femurs. Trabecular number and bone volume/tissue volume both increased (*: $p<0.05$)

A)

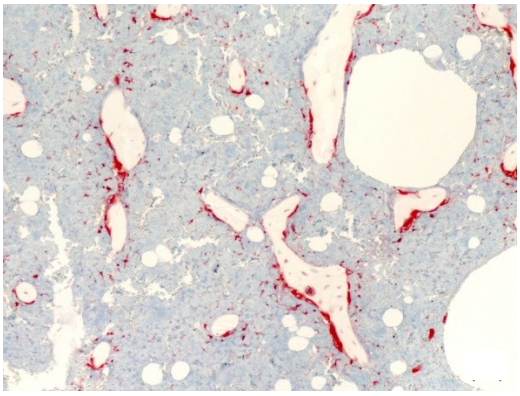

STAT3

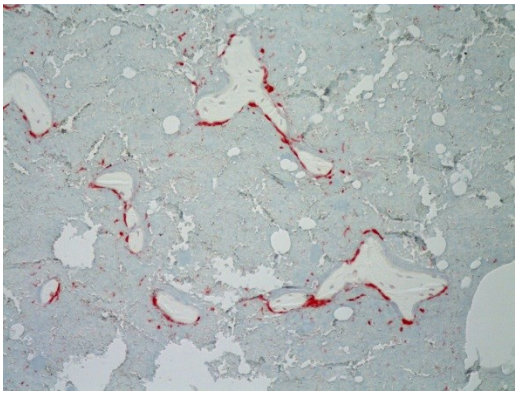

WT

B)

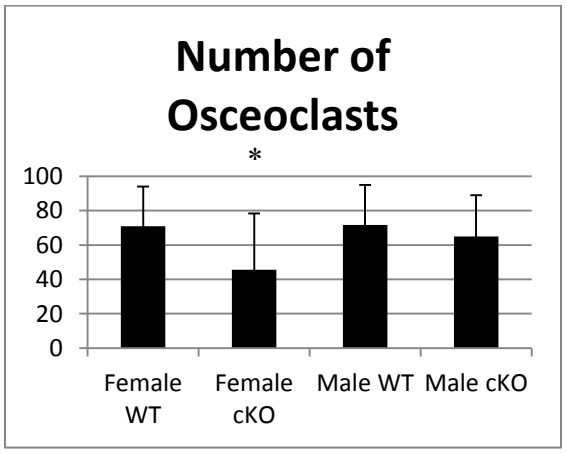

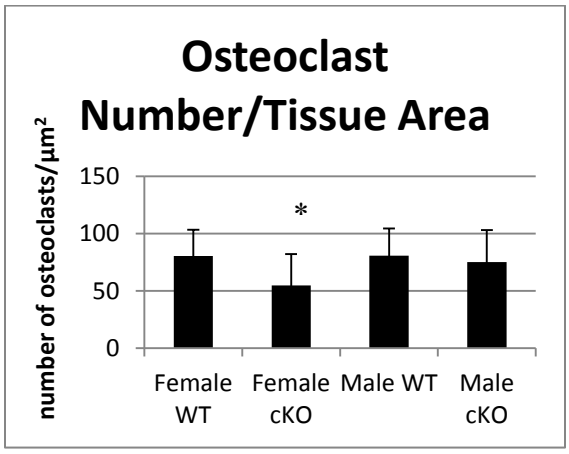

Figure 17: TRAP stain CTSK specific STAT3 KO mice. TRAP stain of female distal femur (A) and graphical representation of data (B) Data was collected from a region 0.8mm proximal from the growth plate of the right femur. Osteoclast number and osteoclast number/tissue area decreased in cKO females (*: $p<0.05$)

A)

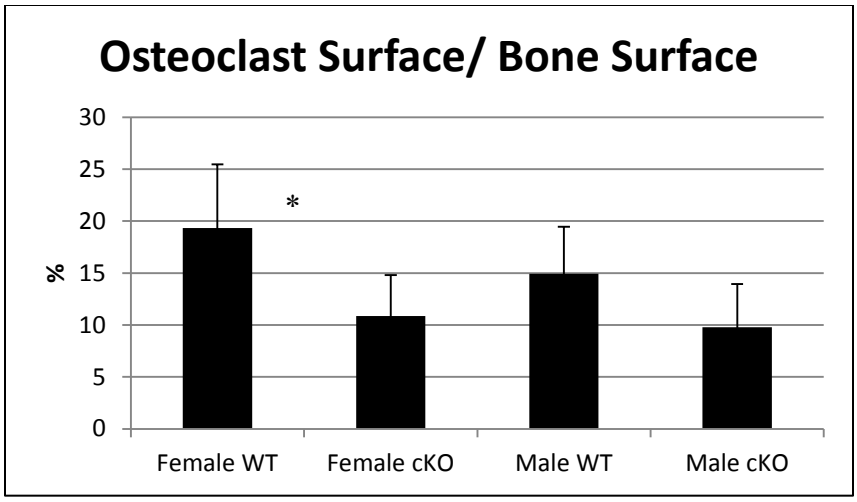

B)

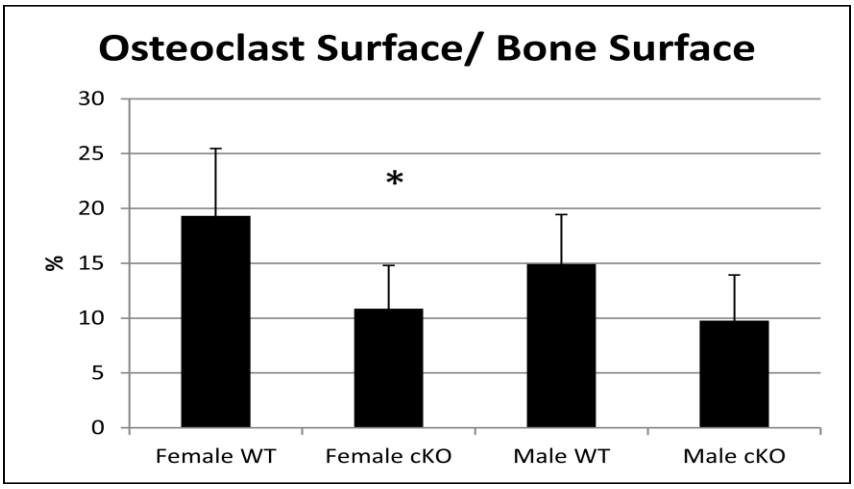

Figure 18: TRAP stain TRAP specific STAT3 KO mice. TRAP stain of right femur from 8 week old TRAP specific STAT3 KO mice. Data was collected from a region 0.8mm proximal from the growth plate of the right femur. Osteoclast number and osteoclast number/tissue area decreased significantly in cKO females compared to controls (*: $p<0.05$)

A)

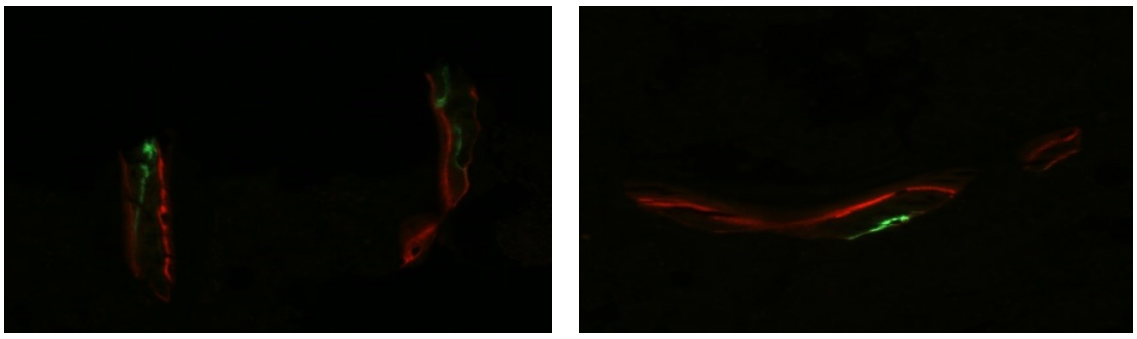

B)

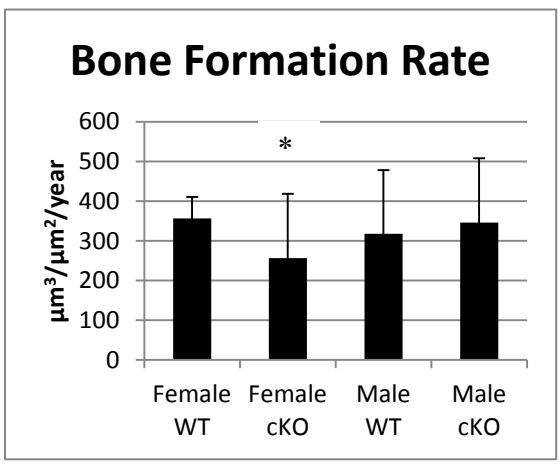

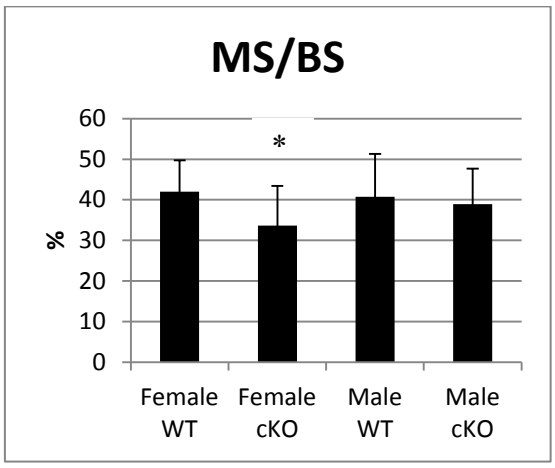

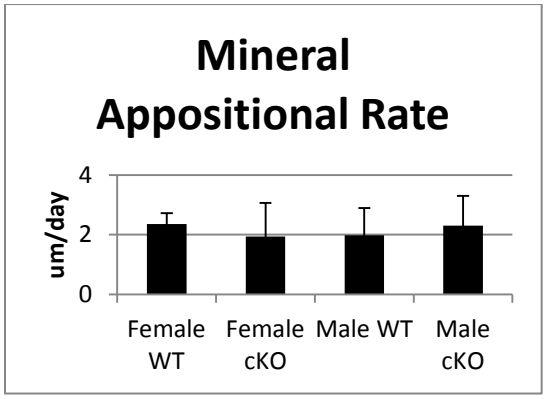

Figure 19: Dynamic histomorphometry CTSK mice. Dynamic histomorphometry from the distal femur of female CTSK STAT3 WT (left) and KO (right) mice (A) and graphical representation of data. Data were collected from a region 0.8mm proximal from the growth plate of the right femur. Calcein and alizarin dyes were injected into the mouse 5 days apart. Bone formation rate and mineralizing surface/bone surface were decreased in cKO females compared to WT females (* $p<0.05$)

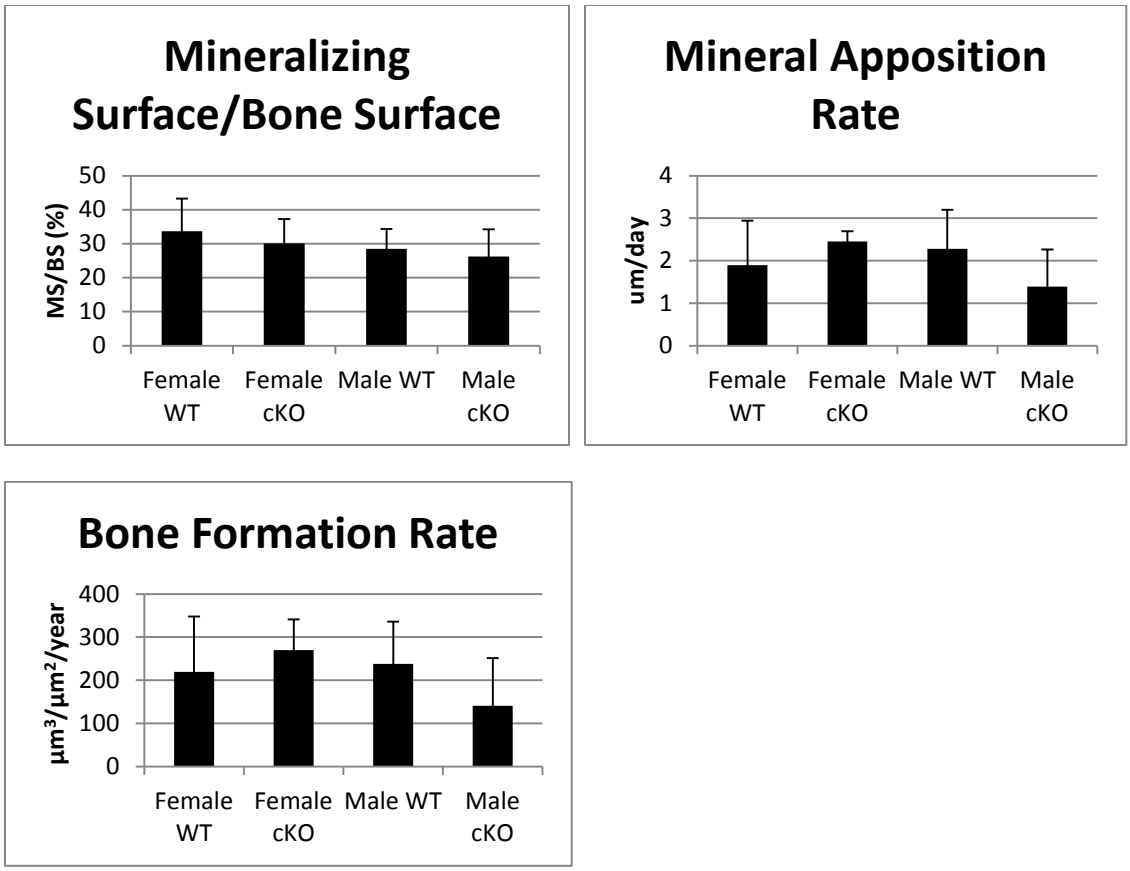

Figure 20: Dynamic histomorphometry TRAP mice. Quantitated data from fluorescent-labeled trabecular bone from right femur of 8 week old TRAP STAT3 WT and cKO mice. Data was collected from a region 0.8mm proximal from the growth plate of the right femur. Calcein and alizarin dyes were injected into the mouse 5 days apart. NO significant differences were detected.

A)

B)

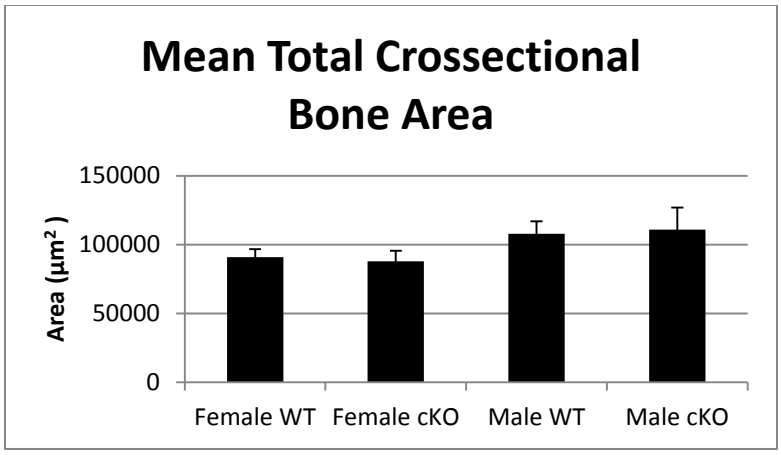

C)

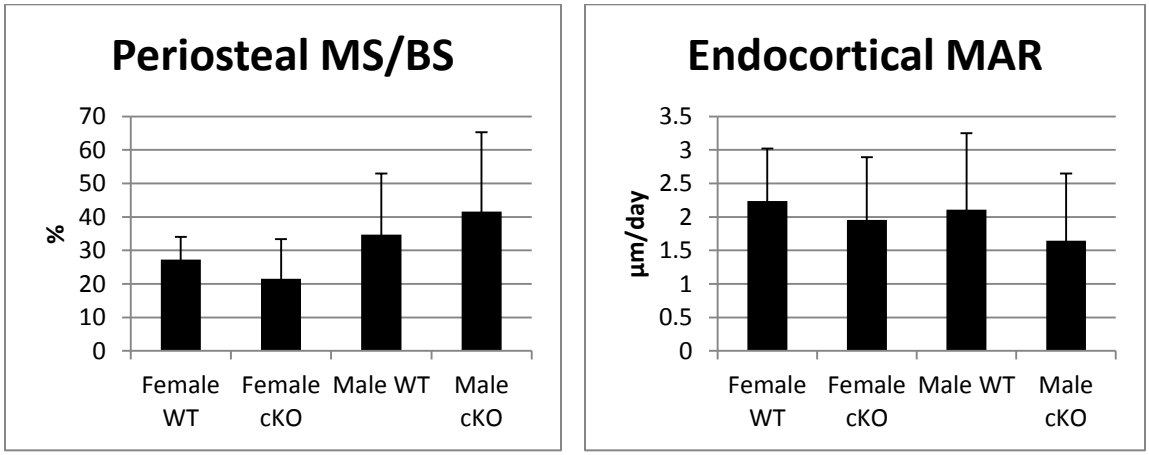

Figure 21: Cortical bone properties 8 week old CTSK STAT3 mice (A) Cortical bone micro CT images from the exact midpoint of the left femur. B) graph of bone area and C) Periosteal MS/BS and endocortical MAR Calcein and alizarin dyes were injected into the mouse 5 days apart. NO significant differences were detected.

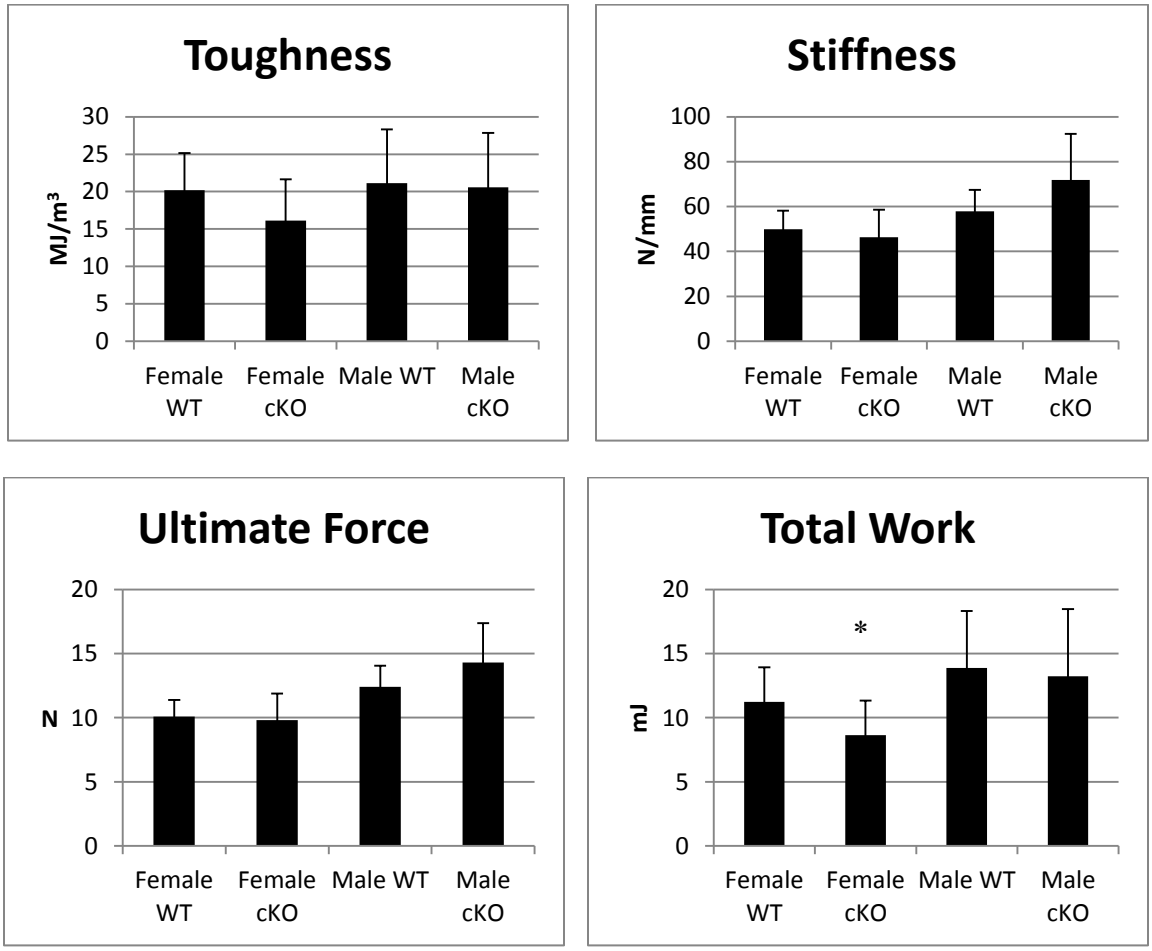

Figure 22: Mechanical testing of CTSK mouse femur. Femurs from 8wk old CTSK STAT3 KO and WT mice were subjected to 3 point bending to determine strength. Left femurs were arranged with anterior side facing downward and loaded with bottom points set 6mm apart with top bending point set in center. A significant difference was detected between WT and cKO female mice in total work (*: $p<0.05$).

A)

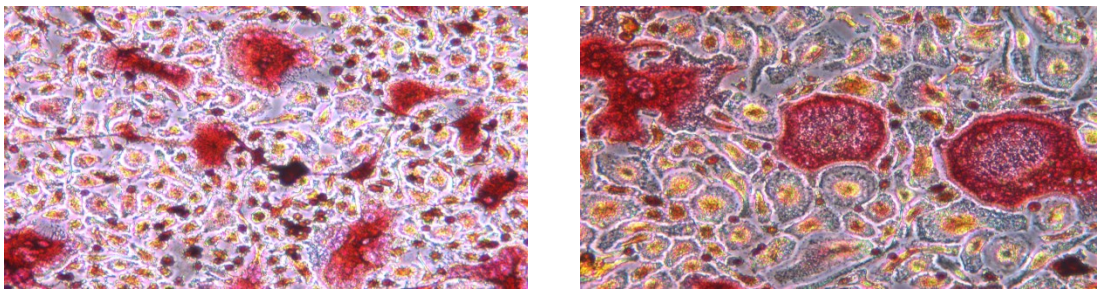

WT KO

B)

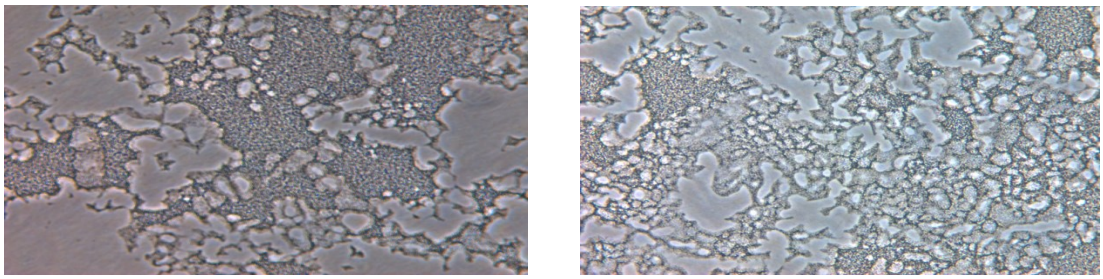

C) WT KO

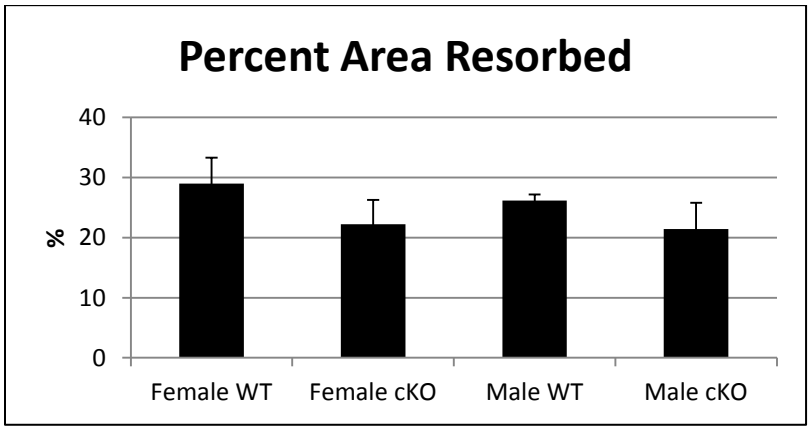

Figure 23: Osteoclast cell culture data. Bone marrow cells were isolated from 6 week old CTSK STAT3 KO and WT mice and were cultured in the presence of RANKL and M-CSF and the number of mature osteoclasts formed as well as the percent of resorbed area was assessed. A) TRAP stained osteoclasts in WT and KO cultures, resorption pit assay B) resorbed surface appears darker than unresorbed surface of osteoassay tissue culture plates, C) qunatitation of the resorption area. N=2 mice pre group. No significant differences were found.